NUMERICAL AND EXPERIMENTAL INVESTIGATION OF RADIAL AND TREE-SHAPED VASCULAR CHANNELS FOR SELF-COOLING STRUCTURES

A Thesis Submitted to
the Graduate School of Engineering and Science of
İzmir Institute of Technology
in Partial Fulfillment of the Requirements for the Degree of

MASTER OF SCIENCE

in Mechanical Engineering

by
Onur YENİGÜN

August 2016
İZMİR

We approve the thesis of **Onur YENİGÜN**

Examining Committee Members:

_____

Assoc. Prof. Dr. Erdal ÇETKİN
Department of Mechanical Engineering, İzmir Institute of Technology

_____

Prof. Dr. Aytunç EREK
Department of Mechanical Engineering, Dokuz Eylül University

_____

Assist. Prof. Dr. Murat Barışık
Department of Mechanical Engineering, İzmir Institute of Technology

4 August 2016

_____

Assoc. Prof. Dr. Erdal ÇETKİN
Supervisor, Department of Mechanical Engineering, İzmir Institute of Technology

_____

Prof. Dr. Figen KOREL
Deputy Head of the Department of Mechanical Engineering

_____

Prof. Dr. Bilge KARAÇALI
Dean of the Graduate School of Engineering and Sciences

ACKNOWLEDGMENTS

First of all, I would like to express my appreciation to my advisor Dr. Erdal ÇETKİN, for his guidance and help throughout this thesis.

I would like to thank TUBITAK for the financial support, under the grant number 114M512.

I also would like to thank my colleagues Tümcan ŞEN, Doğuş ZEREN and Kıvanç TURAN and members of “MiNaEng” Lab. for their friendship and countless times of fun memories. Their presence in my graduate education made everything so much easier.

Last but not least, I take this opportunity to express my gratitude to my family, Cemal, Nurten and Mustafa Can YENİGÜN for their endless care, love and support. They stood by me in every decision I made, gave me courage to step up, help me become the man I am.

ABSTRACT

NUMERICAL AND EXPERIMENTAL INVESTIGATION OF RADIAL AND TREE-SHAPED VASCULAR CHANNELS FOR SELF-COOLING STRUCTURES

In this study, we show experimentally and numerically how a plate which is subjected to a constant heat load can be kept under an allowable temperature limit. Vascular channels in which coolant fluid flows have been embedded in the plate. Three types of vascular channel designs were compared: radial, tree-shaped and their hybrid. The effects of channel design on the thermal performance for different volume fractions (the fluid volume over the solid volume) are documented. In addition, the effects of the number of channels on cooling performance have been documented. Changing the design from radial to tree-shaped designs decreases the order of pressure drop. Hence increase in the order of the convective heat transfer coefficient is achieved. However, tree-shaped designs do not bathe the entire domain. Therefore, additional channels were inserted at the uncooled regions (hybrid design). The best features of both radial and tree-shaped designs are combined in the hybrid of them: the flow resistances to the fluid and heat flow become almost as low as the tree-shaped and radials designs, respectively. Furthermore, this thesis shows how delaying the inlet of the coolant fluid for a given time interval affects the peak temperature. The effect of design on the maximum temperature shows that there should be an optimum design for a distinct set of boundary conditions, and this design should be varied as the boundary conditions change. This result is in accord with the constructal law, i.e. the shape should be varied in order to minimize resistances to the flows.

Keywords and Phrases: Smart materials, Vascularization, Self-cooling, Numerical Simulation, Experimental Study

ÖZET

KENDİNİ-SOĞUTAN YAPILAR İÇİN RADYAL VE AĞAÇ-ŞEKİLLİ VASKÜLER KANALLARIN SAYISAL VE DENEYSEL OLARAK ARAŞTIRILMASI

Bu çalışmada, sabit ısı yüküne maruz kalan bir plakanın, kabul edilebilir bir sıcaklık altında tutulabileceği, sayısal ve deneysel metotlar kullanılarak gösterilmektedir. İçinden soğutucu akışkan geçen vasküler kanallar plakanın içine gömülüdür. Çalışma kapsamında radyal, ağaç-şekilli ve hibrit olmak üzere üç farklı vasküler kanal tasarımı karşılaştırılmıştır. Kanal tasarımının ısıl performans üzerindeki etkisi farklı hacim oranlarında (sıvı hacmin, katı hacme oranı) belgelenmiştir. Ek olarak, kanal sayısının soğutma performansı üzerindeki etkisi incelenmiştir. Radyal tasarımdan ağaç-şekilli tasarıma geçildiğinde basınç düşüşünün azaldığı görülmektedir. Böylece ısı transferi katsayısında yükselme sağlanmıştır. Ancak ağaç-şekilli tasarım bütün gövdeyi soğutamamaktadır. Bu nedenle soğutulamayan bölgelere ek kanallar yerleştirilmiştir (hibrit tasarım). Radyal ve ağaç-şekilli tasarımların en iyi özellikleri hibrit tasarımda toplanmıştır. Sıvı ve ısı akışına karşı gelen dirençler sırasıyla ağaç-şekilli ve radyal tasarımlar kadar düşük olarak belirlenmiştir. Bu tezde soğutucu akışkan geciktirildiğinde, maksimum sıcaklığın nasıl etkilendiği de gösterilmiştir. Tasarımın en yüksek sıcaklık üzerindeki etkisi, farklı sınır koşulları için optimum tasarım olması ve bu tasarımın sınır koşulları ile birlikte değişmesi gerektiğini göstermektedir. Bu sonuçlar yapısal gelişim yasası ile uyumlu olup, şeklin akışa karşı gelen dirençleri düşürecek şekilde değişmesi gerektiğini ortaya koymaktadır.

Anahtar Kelimeler ve Deyimler: Akıllı Malzemeler, Vaskülerizasyon, Kendini-soğutma, Sayısal simülasyon, Deneysel çalışma

TABLE OF CONTENTS

LIST OF FIGURES

Figure **Page**

LIST OF TABLES

Table **Page**

LIST OF SYMBOLS

c_p	Specific heat at constant pressure	J/(kgK)
d	Vascular channel diameter	m
k_f	Thermal conductivity of the fluid	W/(mK)
k_s	Thermal conductivity of the solid	W/(mK)
L	Width of the vascular plate	m
$L_{channel}$	Length of distributing/collecting channel	m
$\dot{m}$	Mass flow rate	kg/s
n	Vector normal to the fluid-solid interface	
P	Pressure	Pa
q''	Heat flux	W/m^2
Re	Reynolds number	
T	Temperature	^oK
t	Time	s
t_d	Time delay	s
u, v, w	Velocity components corresponding to the spatial coordinates	
$\dot{V}$	Volumetric flow rate	m^3/s
x, y, z	Spatial coordinates	

Greek Letters

ΔP	Pressure drop	Pa
φ	Volume fraction	
μ	Dynamic viscosity	kg/(ms)
ν	Kinematic viscosity	m^2/s
ρ	Density	kg/m^3

Subscripts

0, 1, 2, 3	Index of tree branches
I	Index
max	Maximum
min	Minimum
peak	Peak

Superscripts

n	Index of mesh independency test

CHAPTER 1

INTRODUCTION

Advanced technologies require great volumetric cooling capability, especially in miniature designs, according to Cetkin and Oliani (Cetkin and Oliani, 2015). Heat transfer surface area is limited in miniature designs, so they cannot be cooled down with natural or forced convection when working fluid is air. Therefore, the current literature focuses on heat transfer enhancement methods such as phase changing materials or forced convection with working fluids as nano-fluids (Minea, 2015; Shafahi et al., 2010; Ma et al., 2015). These methods are essential in order to increase heat transfer rate. However, heat load can be of two kinds: deterministic and random (Cetkin et al., 2012). The heating rate and the surface on which the heat flux is applied is known in deterministic heating loads such as electronic circuits. In random type loads, neither heating rate nor its surface are known such as thermal runaway phenomenon in accumulators. Advanced technologies require miniature structures with the capability of cooling itself under deterministic and random heating loads. This requirement can be satisfied with self-cooling structures.

Materials with smart features first suggested by White et al. (White et al., 2001). They mimicked the self-healing mechanism of animals, i.e. clot occurrence at the wound in order to seal it. In their autonomic healing concept, healing agents were placed in spheres which can be used once. Later, Bejan et al. (Bejan et al., 2006) discussed that circulating healing agents in embedded vascular channel network enables structure to heal itself countless time. Kim et al. (Kim et al., 2006) showed that vascularized structures can also be used to cool a domain on which heat load applied. Cetkin et al. (Cetkin et al., 2012) uncovered that vascularization provides required cooling for both deterministic and random heat loads. Wang et al. (Wang et al., 2009) uncovered how the mechanical strength of a vascular domain varies with changing the channel design and volume fraction. Cetkin et al. (Cetkin et al., 2015) also showed how vascularization can increase the mechanical strength of a heated domain and when the effect of thermal stresses can be neglected.

Here we show experimentally and numerically how a solid structure can be gained self-cooling capability with minimum energy consumption, i.e. minimum pumping power requirement. The literature is lack of experimental results on self-cooling structures. This study fills the gap. In addition, a hybrid of radial and tree-shaped channel configuration is introduced in order to decrease the fluid flow and heat flow resistances by following the principles of Constructal Law, which is a physical phenomenon that states a flow system should evolve freely in order to adapt the changing conditions (Bejan, 1996). Hence, the peak temperature can be kept under the ceiling value with predictable and random heating loads. Last, vascularized structures are proposed as adjunct to the phase changing materials and nano-fluidic cooling methods, not to replace them.

1.1. Constructal Law

The Constructal law is a law of physics that focuses on generation of flow architecture, structure and geometry. Best way to describe it is to quote from Prof. Bejan, "for a finite-size system to persist in time (to live) it must evolve such that it provides greater and greater access to the currents that flow through it." (Bejan, 1997, p. 815).

The Constructal law brings animate and inanimate designs together in a wide range of examples, such as; delta of a river basin and a cast of a human lung. As shown in Figure 1.1, both designs have the similar flow configurations; dendritic. Though, it is not a coincidence that they both have the similar design, it is the product of evolution in time. Both designs are evolved in a way that the flows experience smallest possible resistances while the circumstances are changed. As explained previously in Prof. Bejan's statement, these designs also change in time for any time the resistances to the flow is always smallest. The examples to the constructal law can be expanded to lightning, vascularized living tissue, nervous system, city traffic, snowflakes etc.

The Constructal law approaches to the design as a phenomenon of physics, the shape and structure of a flow system is a product of systematic progression of minimizing the resistances. The Constructal law changes the perspective of design in modern technology, because the current designs are product of chance, experience, inspiration or art. With engineers following the principles of Constructal law, the designs in modern technology can evolve. Some of the applications of the constructal law in flow systems are documented in the following section.

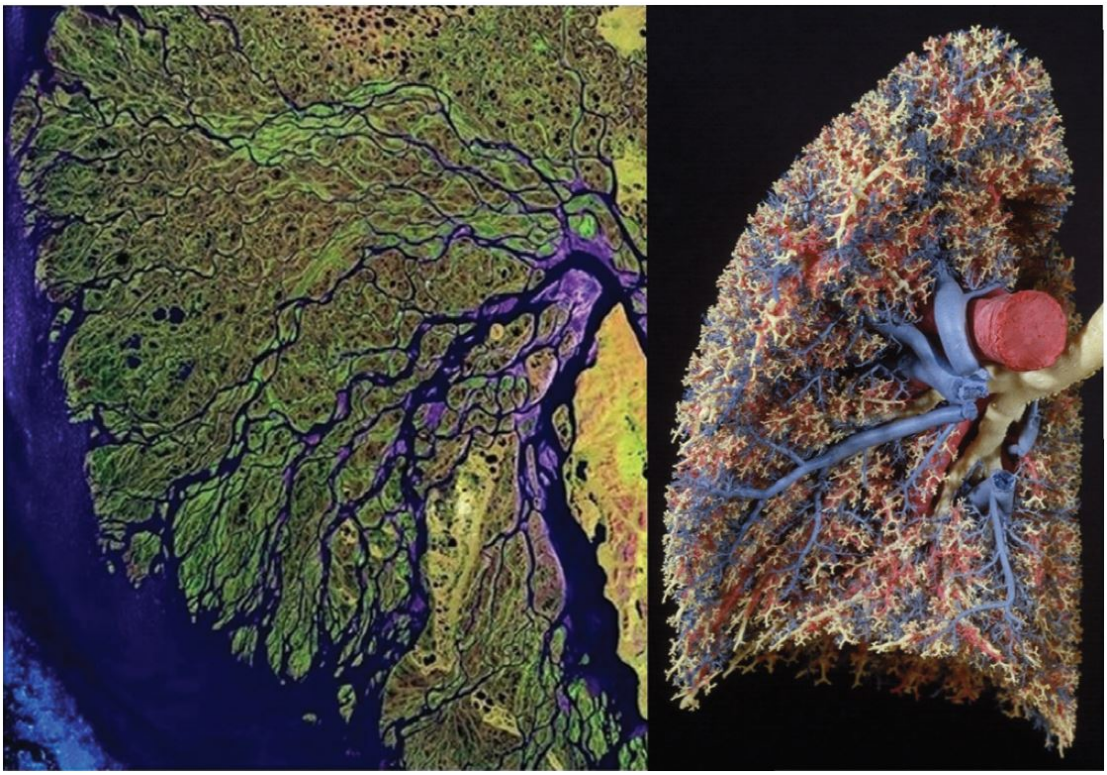

(a) (b)

Figure 1.1. Flow configurations of (a) delta of a river basin and (b) cast of a human lung (Source: Bejan and Lorente, 2013)

1.1.1. Tree Networks

The objective of the tree-shaped network is to distribute (or collect) the flow from one point (source or sink) to an area (or volume) with minimum global resistances to the flow. There are two flow mechanisms for tree-shaped configuration; flow across the channels and diffusion across the spacing between the channels. In order to decrease the global resistances, the spacing between the trees and the diameter ratio at the junctions should be balanced (Bejan and Lorente, 2008).

To generate a tree-shaped configuration, as shown in Figure 1.2, for a flow system with minimum flow resistances, the optimal channel diameter (equation 1.1) and length (equation 1.2) ratios can be used as Hess-Murray Rules states in literature (Bejan and Lorente, 2008). In addition, if a mother channel gives birth to n number of daughter channels, then 2 of Eq. (1.1) should be replaced with the number of channels at the junctions.

$$D_i / D_{i+1} = 2^{1/3} \tag{1.1}$$

$$L_i / L_{i+1} = 2^{1/3} \tag{1.2}$$

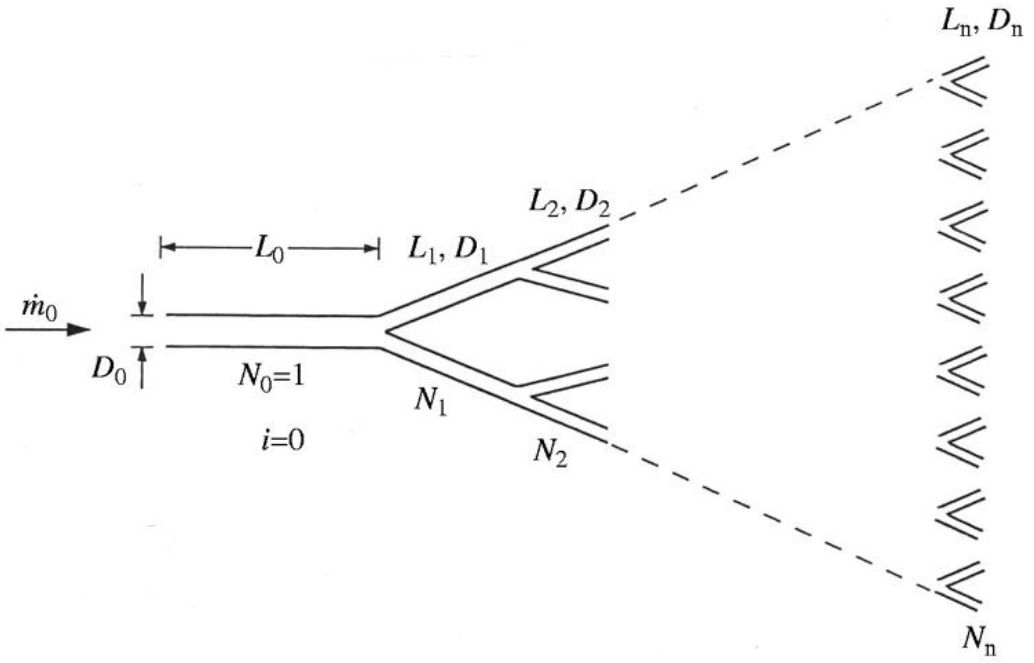

Figure 1.2. Tree-shaped configuration
(Source: Bejan and Lorente, 2006)

Use of tree-shaped networks for flow distribution is a trending topic in modern technology. Bejan and Lorente (Bejan and Lorente, 2008) suggested that using tree-shaped vascular channels in turbine blades, as shown in Figure 1.3. This would increase the lifetime of the blades as cooling gasses circulate in the internal cooling channels of the blade will also infiltrates through the walls via embedded vascular channels close to the surface, where great amount of heat flux is subjected. In addition, tree-shaped configurations are proved to be useful for entropy generation minimization by Sciacovelli and Verda (Sciacovelli and Verda, 2011) in Molten Carbonate Fuel Cells (MCFC). Furthermore, for conduction heat transfer enhancement in heat generating bodies as high conductivity pathways (Kobayashi et al., 2013), Fig. 1.4, tree-shaped configurations are used. Another application of tree-shaped designs in the literature is channel shape optimization of self-cooling structures (Kim et al., 2008). The examples of applications can be expanded to design of photovoltaic cells (Morega et al., 2006), micro-channel heat sinks (Bello-Ochende et al., 2007) and heat exchangers (Raja et al., 2008).

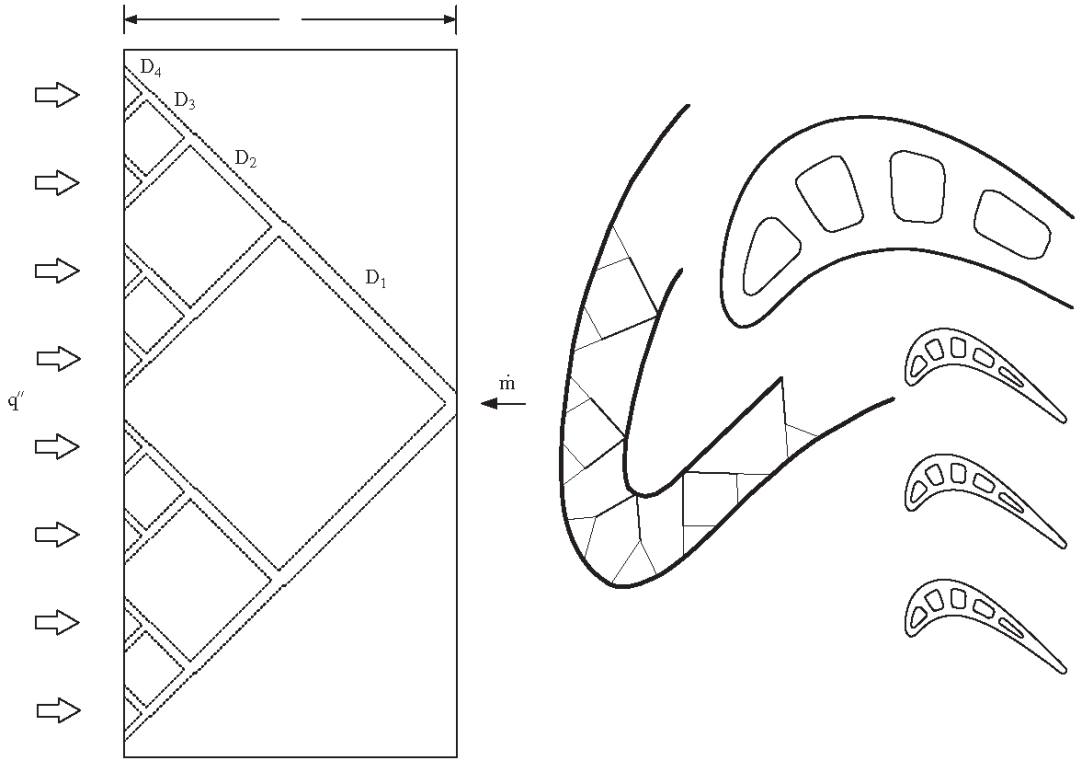

Figure 1.3. Walls of turbine blades with vascularized tree-shaped flow structures (Source: Bejan and Lorente, 2008)

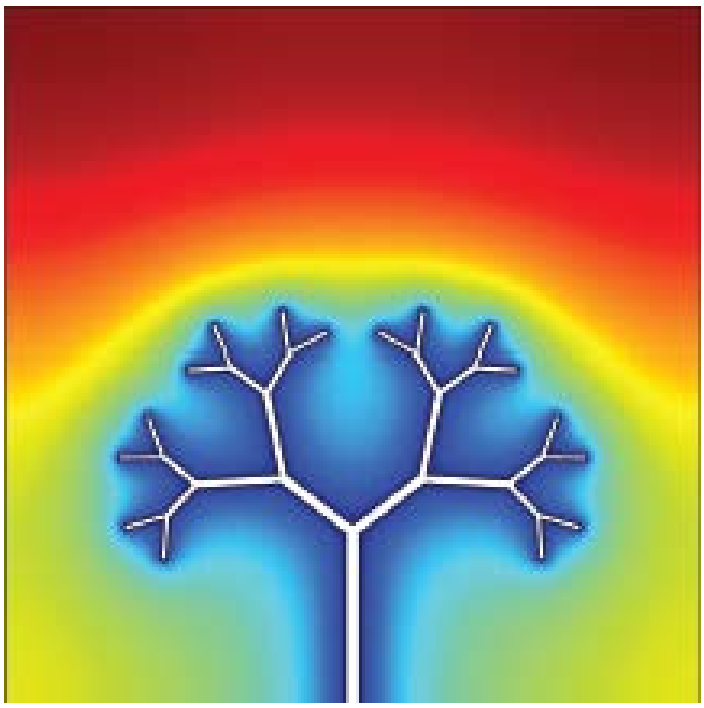

Figure 1.4. Tree-shaped conducting body invading heat generating domain (Source: Kobayashi et al., 2013)

1.2. Smart Materials

Smart materials are structures that have gained artificial features such as self-healing and self-cooling. The common characteristic of these smart materials is that they are mimicked from nature, such as clot appearance in the wound in order to seal it (White et al., 2001) or an embedded circulatory system (Therriault et al., 2003) to distribute fluid with possible repairing or cooling particles. Even though the smart materials are considered under two subcategories; self-healing and self-cooling, there are more features in the literature. Regaining electrical conductivity, enhanced mechanical performance or reducing thermal stresses are some of the features that studied under these two subcategories.

1.2.1. Self-healing Materials

In nature, it is common to have self-healing mechanism in order to survive, increase the lifetime or adapt to the environment, for all creatures. For years, scientists and engineers have tried to adapt this mechanism into the materials that used in mechanical systems such as aerospace or automobile industries, in order to increase the lifetime of these structures or gain some additional functionalities.

Self-healing materials are first introduced to the literature by White et al. (White et. al., 2001). Self-healing materials are developed against micro cracks and hidden damages occurred in structural polymers. In structural polymers, it is hard to detect and repair the micro cracks or hidden damages occurred in the structure. In the study, microencapsulated healing agents are embedded inside the polymer composites, as shown in Figure 1.5. When micro cracks developed through these capsules, healing agents are released and fill the micro cracks with capillary action. In order to polymerize the healing agents, catalyst materials are also embedded inside the composite. It was documented that these microencapsulated healing agents help to composite materials to regain their mechanical performances up to 70%. The advantage of the microencapsulated healing agents is that they are triggered by damage, so it is site-specific. But this self-healing mechanism has practical limitations, such as it is only applicable to polymer composites and microcapsules can only be used once.

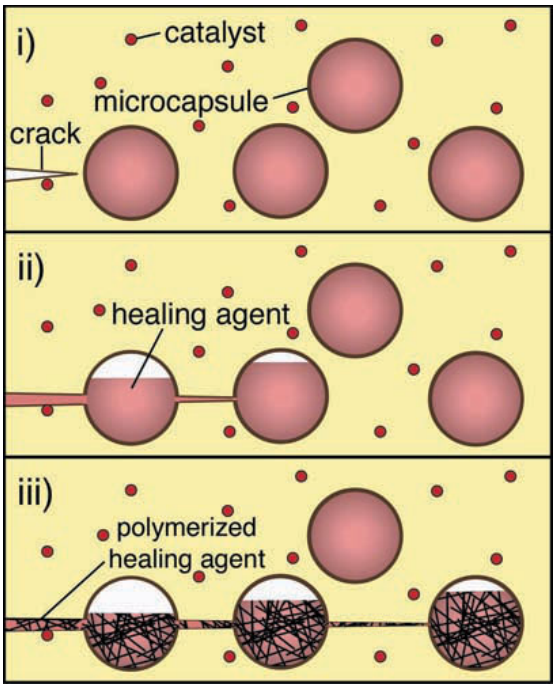

Figure 1.5. The autonomic healing concept
(Source: White et al., 2001)

One time healing of cracks is not a practical approach for mechanical systems. The desire is to gain countless times of healing ability to the smart materials. One way to gain countless times of healing ability is embedding vascular channels inside the structure, as in circulatory system in warm blooded animals. Even though, Therriault et al. (Therriault et al., 2003) first embedded a microvascular channel network inside a composite material, the use of network was for microfluidic mixing. It was Bejan et al. (Bejan et al., 2006) who suggested vascularizing the structure for self-healing ability, as shown in Figure 1.6. In Figure 1.6, a grid-like channel network filled with healing fluid, embedded in a structure is illustrated, with a crack located in the middle. The purpose of the study was to investigate the channel configurations, in order to find the optimal configuration for given conditions, which provides fastest delivery of healing fluid to the crack area. It was stated that in order to have faster fluid delivery, the channel diameters of grid design has to be different, in fact there has to be a ratio between the channel diameters. Kim et al. (Kim et al., 2006) discussed the same problem with tree-shaped channel configurations, in order to distribute the fluid to the entire domain with less pumping power.

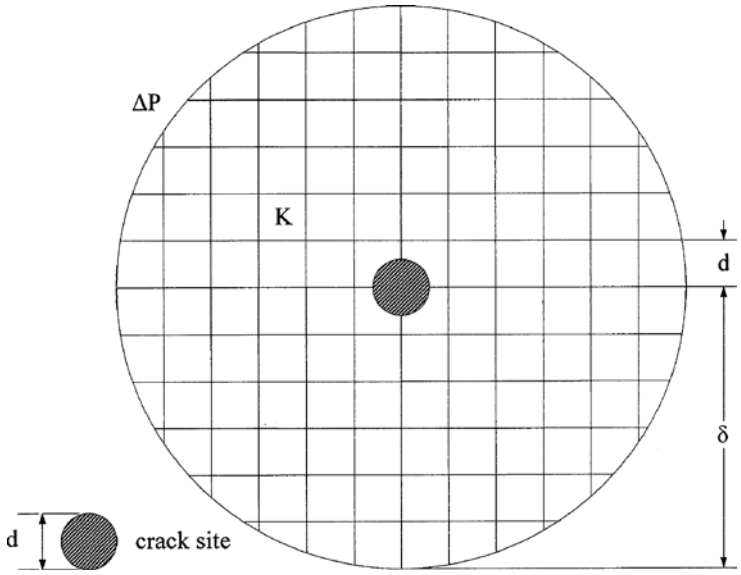

Figure 1.6. Vascularized structure for self-healing
(Source: Bejan et al., 2006)

Toohey et al. (Toohey et al., 2007) studied the use of microvascular channels for self-healing, experimentally. A microvascular channels of network is embedded inside a polymer composite with epoxy coating on top of it as shown in Figure 1.7 (a). Catalyst material is distributed in the epoxy coating and the microvascular channels are filled with the liquid with healing agents. Therefore, if there is a crack in the surface, healing agents move through the vascular channels to the crack site, which can be seen in Figure 1.7 (b), with capillary action, i.e., there is no need for external pressure to move the healing agents. Since the healing agents in the channels and the catalysts are limited and there is no way to re-supply them into the composite material, structure losses its ability to heal itself after repeated self-healings. In the study (Toohey et. al., 2007), maximum 7 repeated healing cycle is achieved with optimizing the catalyst quantity. In addition, containing the catalyst material only in the epoxy coating makes it impossible to heal the cracks formed inside the structure, even if the healing agent reaches to the crack, there will be no catalyzer to polymerize it.

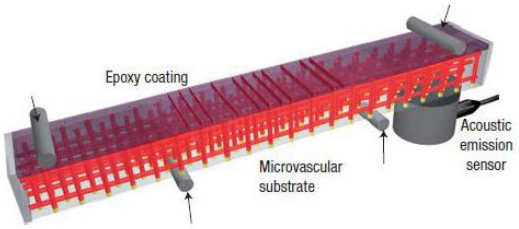

(a)

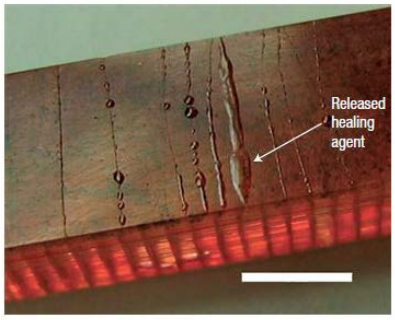

(b)

Figure 1.7. Vascular healing concept; (a) schematic of suggested self-healing concept, (b) image of self-healing structure that shows recovered crack
(Source: Toohey et al., 2007)

Self-healing ability in smart materials also gained restoration of electrical conductivity in the study of Odom et al. (Odom et al., 2012). Same approach in the study of White et al. (White et al., 2001) was used to obtain such a material; carbon nanotubes inside of microcapsules were embedded inside the material and upon fracture, they are released to fill the gaps that opens in gold lines to restore the electrical conductivity.

1.2.2. Self-cooling Materials

Similar to self-healing mechanism, self-cooling is also mimicked from the nature in order to increase lifetime of structures that are subjected to heat loads. Great volumetric heating loads can cause materials to suffer from thermal fatigue which leads to structural breakdown. A structure can be gained self-cooling capability with embedded vascular channels.

Kim et al. (Kim et al., 2006) first suggested that vascularized structures can also be used for self-cooling applications. In this study, canopy to canopy flow configurations as shown in Figure 1.8, were analytically investigated, in order to find global fluid flow resistances. As a result the coolant fluid can bathe the entire volume.

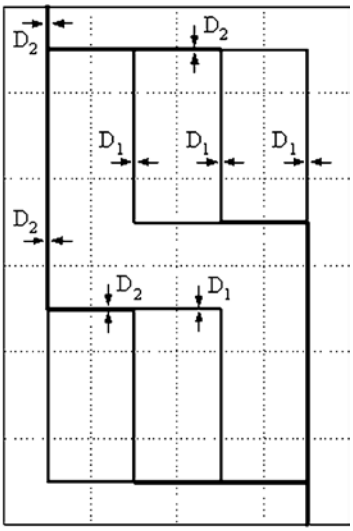

Figure 1.8. Canopy to canopy flow architecture
(Source: Kim et al., 2006)

Lee et al. (Lee et al., 2007) investigated diagonal and orthogonal vascularized channels which can be used for self-cooling. In that study, global resistances to the fluid flow were calculated analytically and optimized by letting the shape morph freely.

Kim et al. (Kim et al., 2008) studied the configuration of transverse trees with different bifurcation levels for self-cooling of a solid body that is exposed to a heat load from one of its surface as shown in Figure 1.9. In the study, it was documented that tree-shaped configurations performs better by means of pressure drop. It was indicated that as boundary conditions change, best design configuration also changes.

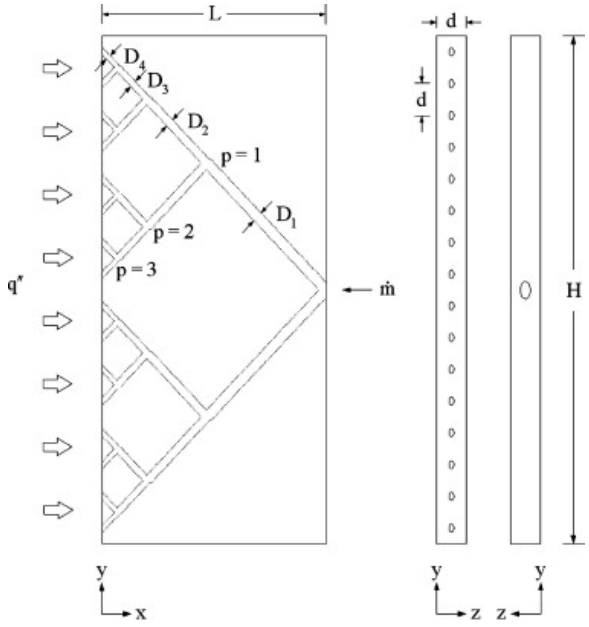

Figure 1.9. Tree-shaped flow structure for self-cooling application
(Source: Kim et al., 2008)

Wang et al. (Wang et al., 2009) presented grid and radial patterns for vascular self-cooling structures. They investigated two inlet/outlet flow configurations for both patterns. The first one is the flow inlet from the center (point to area) of the square slab and the second one is the flow inlet from the channels that located outside (area to point) of the square slab as shown in Figure 1.10. Their results show that center flow inlet have lower global flow resistances than in outside flow inlet, for both design configurations. In addition, for lower peak temperature case, best design changes as the constraints change.

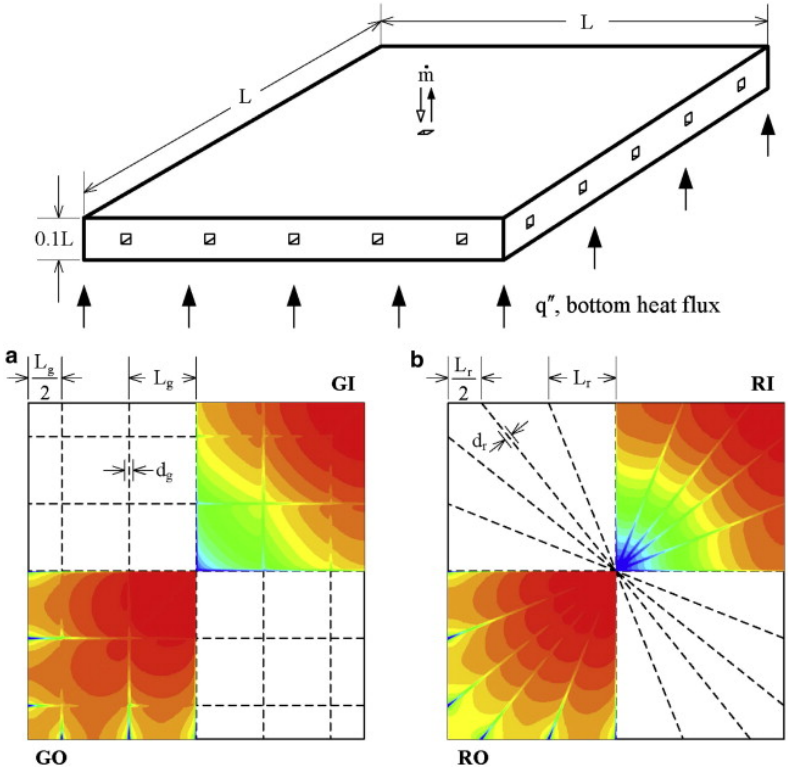

Figure 1.10. Self-cooling structure with (a) grid channel configuration (b) radial channel configuration (Source: Wang et al., 2009)

Lee et al. (Lee et al., 2009) performed a transient study of tree-shaped vascular channels for self-cooling body. Unlike the literature at the time, the heat load was supplied from the below surface not from the side surface. In addition, the flow distributed from point to area but it also collected from the area to a point. Lee et al. also investigated that when the structure should start cooling itself in order to temperature of structure to stay below an allowable limit as the plate subjected to a heat load.

Rocha et al. (Rocha et al., 2009) numerically analyzed the thermal performance of radial and tree-shaped vascular channel configurations for self-cooling structures. An

elemental part of a larger structure was used as the solution domain, Figure 1.11. The center flow inlet configuration was used in this study and the heat load was applied from bottom surface as shown in Figure 1.11. Different volume fractions and number of channels were investigated for both channel design. They concluded that there is no superior design, there is a transition between best designs for different boundary conditions.

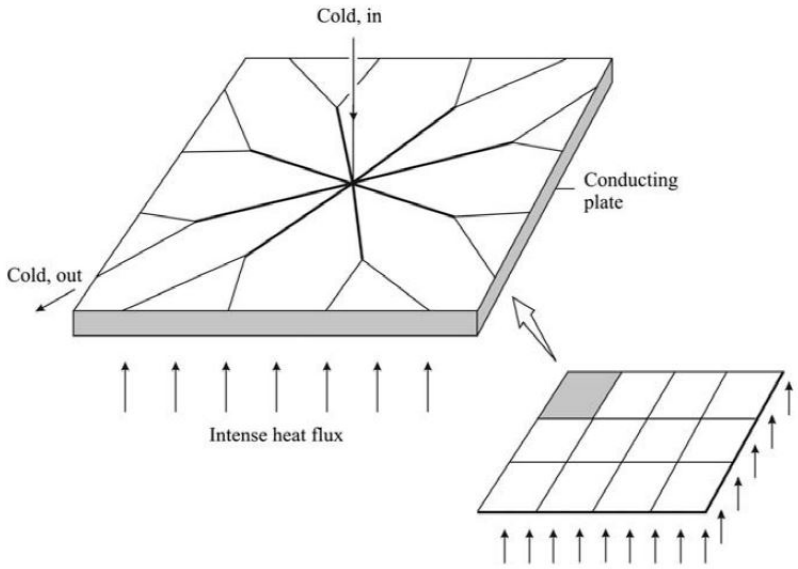

Figure 1.11. Tree-shaped self-cooling structure as elemental part of a larger body (Source: Rocha et al., 2009)

Development and comparison of radial and canopy to canopy constructs documented by Cho et al. (Cho et al., 2010) for a square cooling plate. The effects of configuration and number of channels were investigated by means of pumping power and temperature distribution. In addition, their results showed that radial design has lower global resistances than other constructs, when number of channels is 10. However, the fluid flow resistances were smaller in canopy to canopy constructs, when number of channel were increased.

Wang et al. (Wang et al., 2010) proved that vascularizing a structure not only makes it possible to become a self-cooling material but also increases its mechanical strength. Simply, a structure with the same amount of solid material withstands greater mechanical stresses if there are embedded vascular. In the study, radial and tree-shaped configurations with different level of bifurcations and volume fraction were investigated by means of global fluid flow, thermal and mechanical resistances.

Cho et al. (Cho et al., 2011) performed experimental and numerical studies with the same design configurations in their previous study (Cho et al., 2010). However in this study, they used semi-circular cross-sectioned vascular channels instead of circular cross-section. The semi-circular channels were used in this study in order to ease the manufacturing and preparation process of the test samples. Test samples manufactured from AISI 304 plates and the heat flux was supplied with a silicon rubber heater. The coolant fluid selected as DI water.

According to Cetkin et al. (Cetkin et al., 2011a), increasing the mechanical strength of a structure without changing its volume can be achievable by embedding vascular channels into the structure. Embedding vascular channels also protects the structure from thermal stresses, which can be caused by sudden heating loads. In order to investigate fluid, thermal and stress flows in the smart material, two different configuration of vascular channels (radial and tree-shaped) were embedded inside of a circular slab. Flow directions were selected as flow inlet from center and flow outlet from center. They examined different number of channels (from 6 to 32 channels) for radial design and two different bifurcation levels for tree-shaped design. It was concluded that different design configurations performs better for different set of constraints.

Cetkin et al. (Cetkin et al., 2011b) investigated the increase in mechanical strength and cooling performance of vascular structure, similar to their previous study (Cetkin et al., 2011a). In this study, design pattern was selected as hybrid of grid and radial vascular channels, which was embedded into a square slab with two inlet/outlet flow directions. In addition, applying concentrated heat load to a specific area of the body instead of uniform heat load was analyzed. Hybrid structure discussed in this paper is shown in Figure 1.12. In the study, the effect of L_g/L ratio on thermal performance and mechanical strength was also documented.

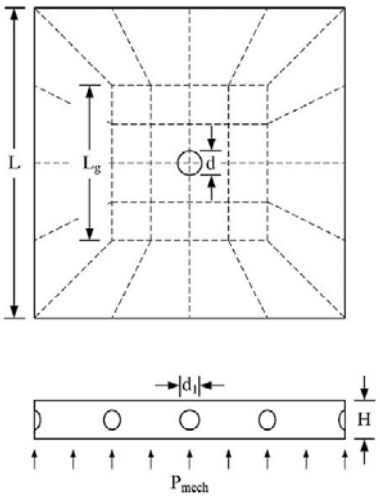

Figure 1.12. Vascular self-cooling structure with hybrid channel of grid and radial (Source: Cetkin et al., 2011b)

Soghrati et al. (Soghrati et al., 2012) discussed that for microvascular channels that cool down a structure with a long distance between its inlet and outlet port is ineffective. According to Soghrati et al., the microvascular channels should redistribute the heat from warmer areas to colder areas. In the study, they embedded sinusoidal microvascular channels from diameter 10μm to 1mm into a 3D glass fiber/epoxy matrix composite as shown in Figure 1.13. They changed the wavelength of the sinusoidal microvascular channels in order to find the optimal channel configuration for certain boundary conditions.

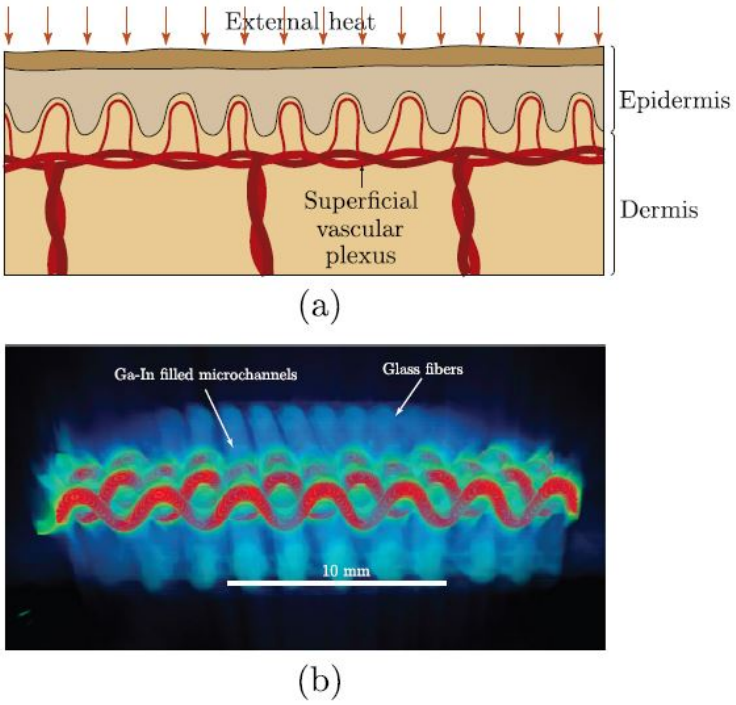

Figure 1.13. (a) Biological and (b) biomimetic schematics of self-cooling application (Source: Soghrati et al., 2012)

In order to investigate the performance of self-cooling structures under random heat loads, Cetkin et al. (Cetkin et al., 2012) studied a vascular structure heated with a randomly moving heat source. In the study, radial, grid and a hybrid of radial and grid vascular channel configurations inserted inside a square plate with two flow directions (inlet in the center and outlet in the center) were investigated. In addition, they investigated the variation of peak temperature in radial design for when the channel diameters are the same and when the flow resistances are the same in all of the channels.

Cetkin et al. (Cetkin et al., 2015) discussed the effect of thermal expansions on vascular structures, which are suitable for structures work under great heat loads, such as turbine blades, engine parts and aerospace applications.

Cetkin (Cetkin, 2015) proposed inserting both high-conductivity materials and vascular cooling channels into a heat generating domain for self-cooling structures, as shown in Figure 1.14. High conductivity inserts discussed in the literature increase overall thermal conductance of heat generating body, with using a stem temperature as a heat sink. In this study, coolant fluid used as a heat sink for high-conductivity inserts. Therefore, high-conductivity inserts addition to vascular cooling channels enhanced the thermal conductance of the body. In addition, this study documented where to place these high-conductivity inserts in the domain.

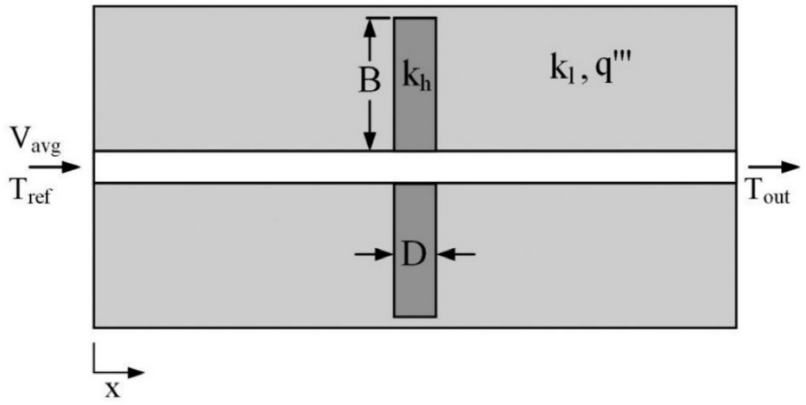

Figure 1.14. Heat generating domain cooled with vascular channel with high-conductivity inserts (Source: Cetkin, 2015)

CHAPTER 2

NUMERICAL MODEL & METHOD

2.1. Numerical Model

Consider a plate with embedded vascularized cooling channels which is subjected to a constant heat flux from one of its surfaces, as shown in Figure 2.1. Coolant fluid flows along the embedded cooling channels. The fluid flow is driven by the pressure difference between the inlet and outlet parts of the vascular network. The volume of the vascular channels and the volume of the solid material are fixed. The outer surfaces of the plate are symmetry boundaries ($\partial \mathrm{T}/\partial \mathrm{n} = 0$) with only exception of the surface on which heat flux is applied, Fig. 2.1. The symmetry condition is selected because the plate is an elemental domain of a system which consists a number of identical elements. The coolant fluid is water and its thermo-physical properties as a function of temperature are given in Table 2.1. In addition, the fluid flow is steady and single phase. With these are in mind, the conservation of mass, momentum and energy equations can be written as

$$\frac{\partial u}{\partial x}+\frac{\partial v}{\partial y}+\frac{\partial w}{\partial z}=0 \tag{2.1}$$

$$u\frac{\partial u}{\partial x}+v\frac{\partial u}{\partial y}+w\frac{\partial u}{\partial z}=-\frac{1}{\rho}\frac{\partial P}{\partial x}+\nu\left(\frac{\partial^2 u}{\partial x^2}+\frac{\partial^2 u}{\partial y^2}+\frac{\partial^2 u}{\partial z^2}\right) \tag{2.2}$$

$$u\frac{\partial v}{\partial x}+v\frac{\partial v}{\partial y}+w\frac{\partial v}{\partial z}=-\frac{1}{\rho}\frac{\partial P}{\partial y}+\nu\left(\frac{\partial^2 v}{\partial x^2}+\frac{\partial^2 v}{\partial y^2}+\frac{\partial^2 v}{\partial z^2}\right) \tag{2.3}$$

$$u\frac{\partial w}{\partial x}+v\frac{\partial w}{\partial y}+w\frac{\partial w}{\partial z}=-\frac{1}{\rho}\frac{\partial P}{\partial z}+\nu\left(\frac{\partial^2 w}{\partial x^2}+\frac{\partial^2 w}{\partial y^2}+\frac{\partial^2 w}{\partial z^2}\right) \tag{2.4}$$

where x, y and z are spatial coordinates, and the velocity components that correspond to these coordinates are u, v and w, respectively. P, ρ and ν are the pressure, density and kinematic viscosity of the fluid.

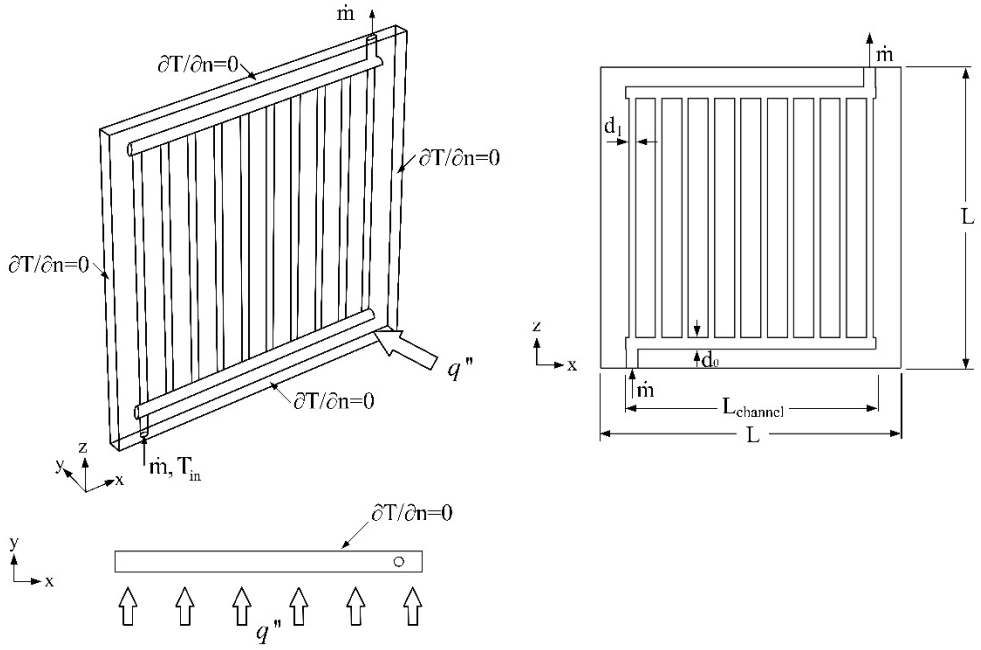

Figure 2.1. The plate with embedded radial cooling channels, boundary conditions with perspective of the geometry and dimensions

The temperature distribution inside the fluid domain is calculated by solving the energy equations,

$$\rho c_p (u\frac{\partial T}{\partial x} + v\frac{\partial T}{\partial y} + w\frac{\partial T}{\partial z}) = \frac{\partial}{\partial x}(\mathrm{k}_f \frac{\partial T}{\partial x}) + \frac{\partial}{\partial y}(\mathrm{k}_f \frac{\partial T}{\partial y}) + \frac{\partial}{\partial z}(\mathrm{k}_f \frac{\partial T}{\partial z}) \qquad (2.5)$$

$$\frac{\partial}{\partial x}(\mathrm{k}_s \frac{\partial T}{\partial x}) + \frac{\partial}{\partial y}(\mathrm{k}_s \frac{\partial T}{\partial y}) + \frac{\partial}{\partial z}(\mathrm{k}_s \frac{\partial T}{\partial z}) = 0 \qquad (2.6)$$

where T is the temperature, c_p and k_f are the specific heat at constant pressure and the thermal conductivity of the coolant fluid and k_s is the thermal conductivity of the solid as given in Table 2.1. The heat continuity in between the solid and fluid domains require

$$k_f \left.\frac{\partial T}{\partial n}\right|_f = k_s \left.\frac{\partial T}{\partial n}\right|_s \qquad (2.7)$$

where n is the vector normal to the fluid-solid interface.

Table 2.1. Thermo-physical properties of DI Water, AISI 304 and Al 5083 at atmospheric pressure

	DI Water (Cho et al., 2011)	AISI 304 (Cho et al., 2011)	Al 5083 (COMSOL Multiphysics)
ρ	998.2	8030.0	2699.5
k	$-0.829+0.0079T-1.04\times10^{-5}T^2$	$11.702649+0.012955T$	$30.01698+0.4662148T$ $-6.570887\times10^{-4}T^2+3.182847\times10^{-7}T^3$
c_p	$5348-7.42T+1.17\times10^{-2}T^2$	$114.227517+1.877902T-0.003234T^2$ $+3.0\times10^{-6}T^3-8\times10^{-10}T^4$	$-263.528+9.293216T-0.01210442T^2$ $-6.74101\times10^{-5}T^3+1.654763\times10^{-7}T^4$
μ	$0.0194-1.065x10^{-4}T$ $+1.489\times10^{-7}T^2$	–	–

2.2. Numerical Method

Consider the square slab of Figure 2.1 with semi-circular vascularized channels embedded inside of it. The volume of the cooling channels and the solid domain (volume fraction, φ) are fixed. In addition, ratio of d_0 over d_1 is also fixed. The vascularized channels are placed in radial form with the total channel volume of $4x10^{-6}m^2$. There are one distributing and one collecting channels with the diameter of $d_0=4.674x10^{-3}m$ and there are ten daughter channels with the diameter of $d_1=2.589x10^{-3}m$. The surface on which the heating load of 5000 W/m^2 is applied shown in Figure 2.1. The coolant fluid enters to the main distributing channel with P_{in} inlet pressure which varies from 30Pa to 3kPa. The outer surfaces of the plate are symmetry boundaries, i.e., $\partial T/\partial n = 0$, except the boundary on which the heating load is applied.

Conservation of mass, momentum and energy equations were solved by using a finite element software (COMSOL Multiphysics 5.0). Mesh elements are non-uniform with boundary layer meshes in order to uncover the effect of sudden changes of the gradients near the boundaries. The mesh size was decreased until the criteria given in equations (2.8) and (2.9) are both satisfied. Relative numerical errors corresponding to the mesh size can be seen in Table 2.2. Table 2.2 shows that the solution becomes mesh independent with 261248 mesh elements.

$$\left|(T_{peak}^{m}-T_{peak}^{m+1})/T_{peak}^{m}\right|<5x10^{-3} \tag{2.8}$$

$$\left|(\dot{m}_{inlet}^{n}-\dot{m}_{inlet}^{n+1})/\dot{m}_{inlet}^{n}\right|<5x10^{-3} \tag{2.9}$$

Table 2.2. Relative numerical errors corresponding to the number of mesh elements

Number of Mesh Elements	T_{peak}[K]	$\left\|(T^{n}_{peak} - T^{n+1}_{peak}) / T^{n}_{peak}\right\|$	$\dot{m}_{inlet}[kg/s]$	$\left\|(\dot{m}^{n}_{inlet} - \dot{m}^{n+1}_{inlet}) / \dot{m}^{n}_{inlet}\right\|$
126385	318.13	-	7.28×10^{-4}	-
187142	317.83	9.43×10^{-4}	7.64×10^{-4}	4.97×10^{-2}
261248	317.59	7.55×10^{-4}	7.67×10^{-4}	3.93×10^{-3}

Then, the simulation results are validated by using numerical and experimental data of Cho et al. (Cho et al., 2011). Figure 2.2 shows that the current study agrees well with the results of Cho et al. (Cho et al., 2011). The change in the mass flow rate is maximum %6.60 and %2.95 for numerical and experimental studies in comparison to Cho et al. (Cho et al., 2011), respectively. In addition, the change in the peak temperatures are 2.14% and 1.23% for pressure drops of 94.8Pa and 277.9Pa for numerical studies documented in Cho et al. (Cho et al., 2011). Therefore, it is concluded that the simulation results are mesh independent and accurate in comparison with the current literature.

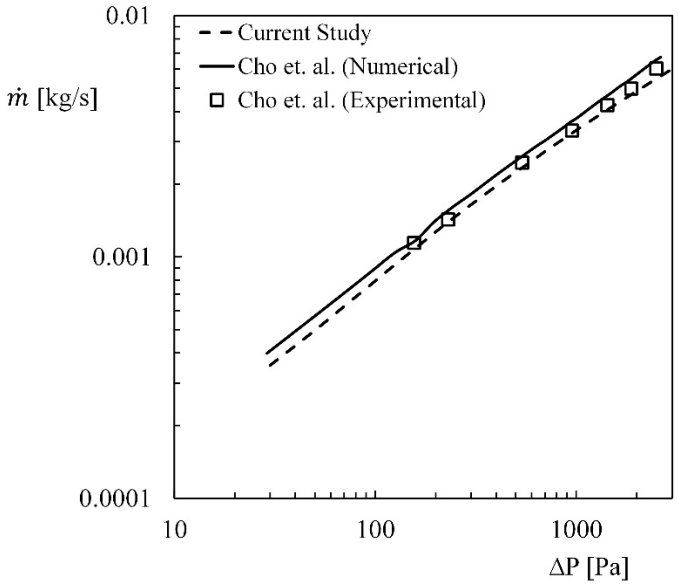

Figure 2.2. Validation of current numerical method

CHAPTER 3

EXPERIMENTAL METHOD

In order to validate the numerical results of vascular self-cooling structures that discussed in this study, an experimental setup is put together and Figure 3.1 shows (a) the schematic and (b) the photograph of the experimental setup. The setup consists of three main parts; circulator cooling bath, test section and data acquisition system. In below sections all of the components of the setup, test samples, procedure and the uncertainty analyses will be explained.

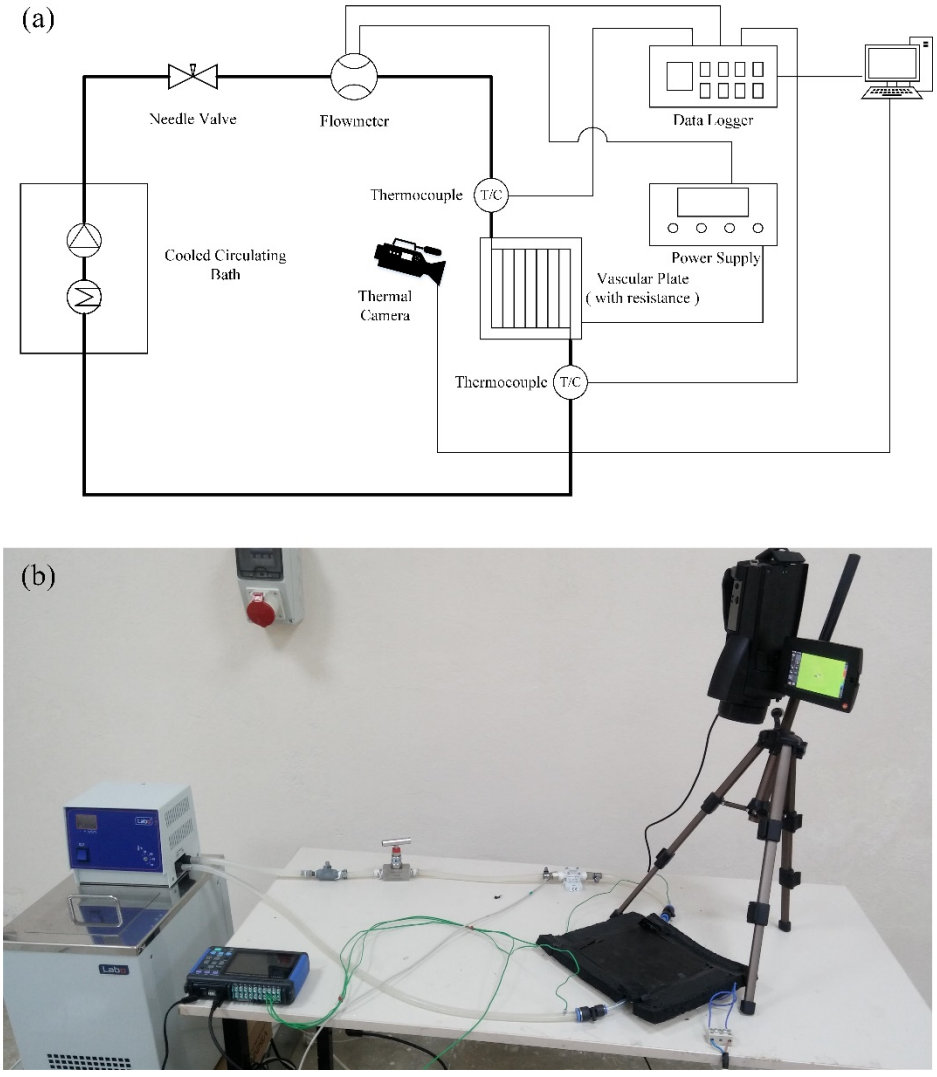

Figure 3.1. (a) The schematic and (b) the photograph of the experimental setup

3.1. Experimental Setup

As shown in Figure 3.1 (a), the experimental setup consists of cooled circulating bath, needle valve, turbine flowmeter, thermocouples, test sample (vascular plate), thermal camera, silicone flexible resistance and data logger. In this section all of the components of the experimental setup will be explained.

3.1.1. Cooled Circulating Bath

Circulatory that showed in Figure 3.2, consists of a heated/cooled bath (Labo C200-H13) with the temperature range of -20/+100°C, the temperature stabilization of ±0.03°C and maximum volumetric flow rate of 13 lt/min. Temperature control of the bath is achieved with a PID control system that embedded in the device.

Figure 3.2. Labo C200-H13 Heated/cooled circulating bath

3.1.2. Needle Valve

Due to its design that allows relatively low flow rates and precise flow regulation, a needle valve (ELX-FF 316ss Needle Valve) that showed in Figure 3.3, is used in the experimental setup. With using the needle valve, volumetric flow rate reduced to range of 0.025 lt/min to 0.40 lt/min from 13 lt/min.

Figure 3.3. ELX-FF 316ss Needle Valve

3.1.3. Flowmeter

A turbine flowmeter (FLOWX3 ULF ultra-low flow sensor) with the flow range of 0.025-1.67 lt/min and with the working temperature of -10°C to 80°C, is inserted in the coolant line, Figure 3.4. The linearity and repeatability of the flowmeter are ±1% and ±0.5% of full scale, respectively. The maximum flow rate in the coolant section is 0.40 lt/min, where it stays in the range of the inserted turbine flowmeter. The signal output of the flowmeter is square wave, which is counted with the data logger. In addition, calibration of the flowmeter is done with bucket and stopwatch method.

Figure 3.4. FLOWX3 ULF ultra-low flow sensor

3.1.4. Thermocouples

Temperature of the ambient and coolant at the inlet and outlet of the vascular plate are measured via K-type thermocouples. These thermocouples are consists of NiCr (+) and NiAl (-) conducting wires with 2x0.50mm diameters and have an accuracy of 0.1°C. In addition, the positions of thermocouples in the inlet and outlet channels are changed in

vertical direction in order to confirm that the temperature distribution is uniform in the channels (the temperature differences at the different vertical positions are maximum 0.1°C, hence; the measured temperature is considered as the mean temperature at the inlet and outlet ports.). The accuracy of the thermocouples were also checked by measuring the temperature of a reservoir with known temperature, which is confirmed via mercury-in-glass thermometer.

3.1.5. Test Samples (Vascular Plates)

The vascular plates were manufactured from 170x170mm 5083 Aluminum plates with semi-circular channels on top with precision CNC (computer numerical controlled) milling machine. Afterwards, two Aluminum plates were adhered together with metal epoxy to form the vascular plate, which can be seen in Figure 3.5 (b), along with the open form of the vascular plates, Figure 3.5 (a). In Figure 3.5 (c), vascular plate is coated with black film due to the low emissivity of aluminum, which can cause misreading from the thermal camera.

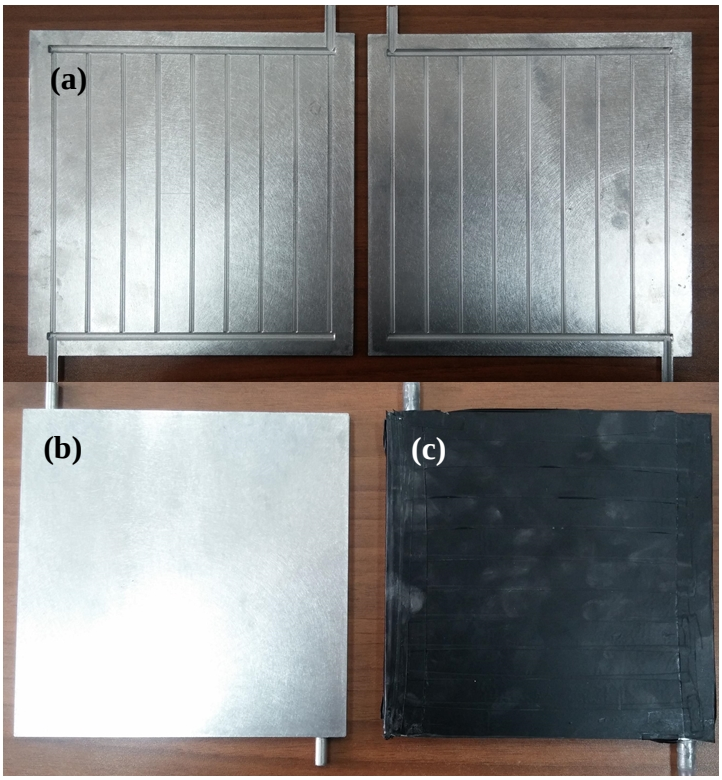

Figure 3.5. Vascular plates (a) open form, (b) closed from, (c) coated form

The vascular plate that shown in Figure 3.5 (a) is in radial channel configuration. There are two more vascular plates with tree-shaped and hybrid channel configuration as test samples, which are given in Figures 3.6 (a) and (b), respectively.

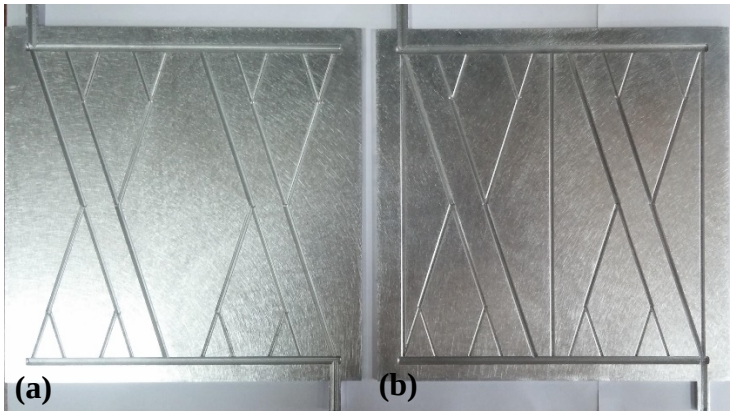

Figure 3.6. Vascular plates with (a) tree-shaped and (b) hybrid channel configuration

3.1.6. Thermal Camera

Figure 3.7 shows the thermal camera (Testo 855-2) that used to capture the temperature distribution of the top surface of the vascular plate. The thermal camera has three measurement ranges; -20 to 100°C, 0 to 350°C and 350 to 1200°C, with the accuracy of ±2% and reproducibility of ±1% of measured values. In addition, the emissivity/reflected temperature settings are set to 0.96 and the temperature values on the coated vascular plate confirmed with placing thermocouples to specific location on the plate.

Figure 3.7. Testo 855-2 thermal camera

3.1.7. Heater

A silicone flexible resistance with two different power; 50W and 150W is used as a heater to generate a constant and uniform heat flux to the bottom surface of the plate. The silicone flexible resistance is presented in Figure 3.8.

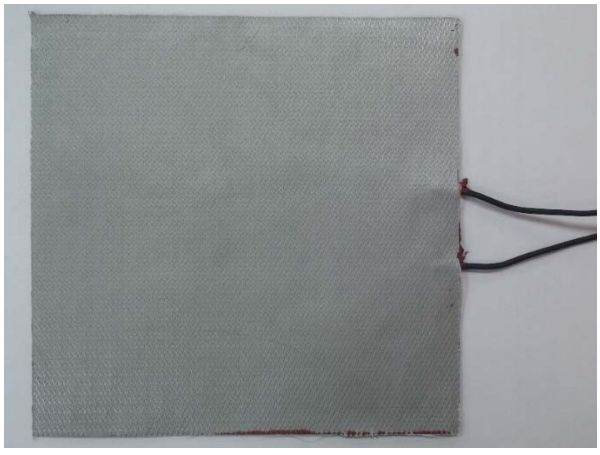

Figure 3.8. Silicone flexible resistance

3.1.8. Data Logger

Flowmeter and the thermocouples that used to measure the temperature of the ambient and coolant at the inlet and outlet of the vascular plate are connected directly to a data logger (Hioki LR8431-20 hi-logger), Figure 3.9, to store and observe the measurements.

Figure 3.9. Hioki LR8431-20 hi-logger

3.2. Experimental Procedure

First, the coolant fluid (distilled water) is cooled down to 20°C in the circulating bath. Then, the silicone flexible resistance is started to heat the vascular plate as the flow adjust to the desired volumetric flow rate and thermal camera turned on. The coolant fluid goes through the needle valve, flowmeter and vascular plate, respectively and then flow back to the circulating bath, where its cooled down to 20°C, again. The procedure is repeated by increasing the volumetric flow rate up to the limit, where Reynolds number reaches critical point for laminar flow and is repeated again by increasing the heat load. In addition, while the experiments were being conducted for a cooling plate, the maximum temperature on the surface of the plate is monitored via thermal camera and the volumetric flow rate, ambient and inlet/outlet water temperatures were stored in the data logger. In addition, these values are also monitored for the time dependency (i.e., when system reaches to steady state conditions).

3.3. Experimental Uncertainties

Detailed uncertainty analysis for measurement instruments and various variables were made according to Figliola and Beasley (Figliola and Beasley, 2011). The propagation of uncertainty method is used,

$$u_R = \left[\left(\frac{\partial R}{\partial x_1} u_1 \right)^2 + \left(\frac{\partial R}{\partial x_2} u_2 \right)^2 + ... + \left(\frac{\partial R}{\partial x_n} u_n \right)^2 \right] \quad (3.1)$$

Where u_R is the uncertainty of $R = R(x_1, x_2, ..., \mathrm{x}_n)$, a functional relationship of independent variables x_n and u_n are the uncertainties of independent variables x_n. Total uncertainties calculated for flowmeter, thermal camera and Reynolds number are ± 3.42%, ±0.62%, and ±3.42%, respectively.

CHAPTER 4

RESULTS AND DISCUSSION

In this chapter, the numerical and the experimental results, along with the design descriptions, are presented for the competing designs: radial, tree-shaped and hybrid designs. Besides the effect of design on self-cooling, the effect of volume fraction and number of channels on peak temperature are also documented.

This chapter splits into two main parts: 120x120mm vascular plates and 170x170mm vascular plates. In 120x120mm vascular plates section, only numerical studies conducted, but in 170x170mm vascular plates section, numerical studies are validated with experimental results.

4.1. 120x120mm Vascular Plates

In this section, the numerical results of self-cooling structures with radial, tree-shaped and hybrid channel configurations are discussed when the plate dimensions are 120x120mm. The effect of design, volume fraction and number of channels on peak temperature of the vascular cooling plate are presented, also temperature distributions are given for each design in order to see if it is distributed evenly. In addition, a time dependent study is conducted and presented for hybrid design.

4.1.1. Radial Design

Consider the radial cooling channel design in Figure 2.1, with 120x120mm AISI 304 stainless steel plates, which is exposed to a heat load of 5000 W/m^2. Figure 4.1 (a) shows that the resistances to the fluid flow decrease by changing only the cross-section of the channels from semi-circular to circular, while the volume fraction (φ) kept fixed. The result of Figure 4.1 (a) was expected because the hydraulic diameter of semi-circular channels is smaller than in the circular channels for the same volume. In addition, Figure 4.1 (b) shows how the peak temperature varies as pressure drop changes for circular and

semi-circular channels. Figure 4.1 (b) shows that the peak temperature decreases as the cross-section is changed from semi-circular to circular channels when the fluid and solid volumes are fixed until pressure drop increases from 30 Pa to 1500 Pa. This design effect is more visible when pressure drop is smaller than 1000 Pa. Until this limit, the drop in the flow resistances provides smaller peak temperatures in circular cross-section channels than in semi-circular ones. However, if pressure drop becomes greater than 1000 Pa, then this effect diminishes as enough coolant is received by the channels for cooling. As pressure drop is kept increased from 1500 Pa to 3000 Pa, semi-circular channels provide slightly smaller peak temperature (% 0.101) in comparison with circular channels. The reason of this is that the radius of semi-circular channels are greater than in circular channels and they have the same point as origin. Therefore, the conductive resistances with circular channel configurations are greater than with the semi-circular channel configurations. The effect of this difference in conductive resistances becomes visible as convective resistances decrease greatly and their order becomes similar to the conductive resistances, i.e. the convective heat transfer coefficient increases due to the increase in pressure drop.

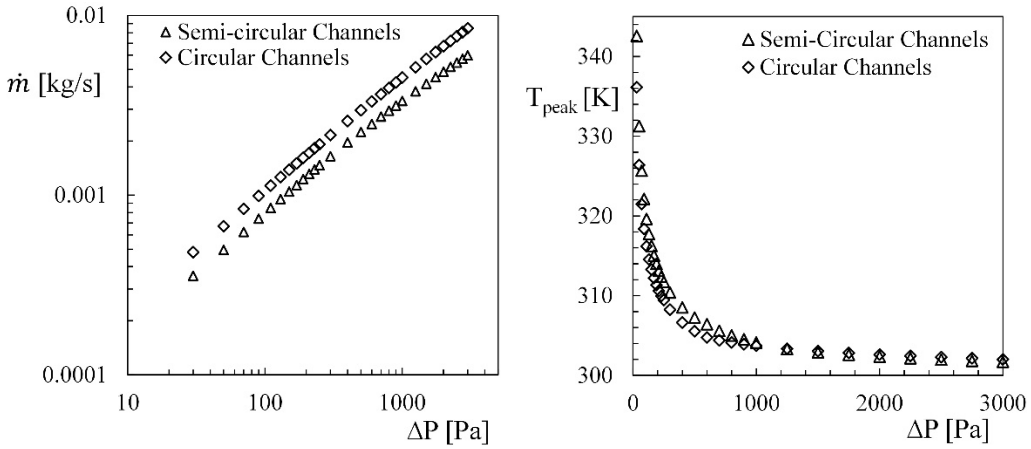

Figure 4.1. (a) Mass flow rate and (b) peak temperature with respect to pressure drop for radial design: semi-circular and circular channels.

Next, the volume fraction (φ) of radial design changes from 0.065 to 0.035, 0.05 and 0.08 in order to uncover the effects of φ on the cooling performance, while the ratio of channel diameters (d_0/d_1) is fixed. Figure 4.2 shows that how the peak temperature varies when pressure drop varies between 30 Pa to 250 Pa for the volume fractions of φ=0.035, 0.05, 0.065 and 0.08. The peak temperature decreases as the volume fraction

increases, Figure 4.2. The reason for this decrease is that the resistances to the fluid flow decreases as channel diameters increase, and therefore the fluid gains greater access to the entire domain (i.e., convective and conductive resistances decrease). In addition, the surface area of the cooling channels also increase, which increases the overall heat transfer rate. Similar to Figure 4.1 (b), in Figure 4.2 shows that as the pressure drop increases the peak temperature becomes independent of the changes in the pressure drop.

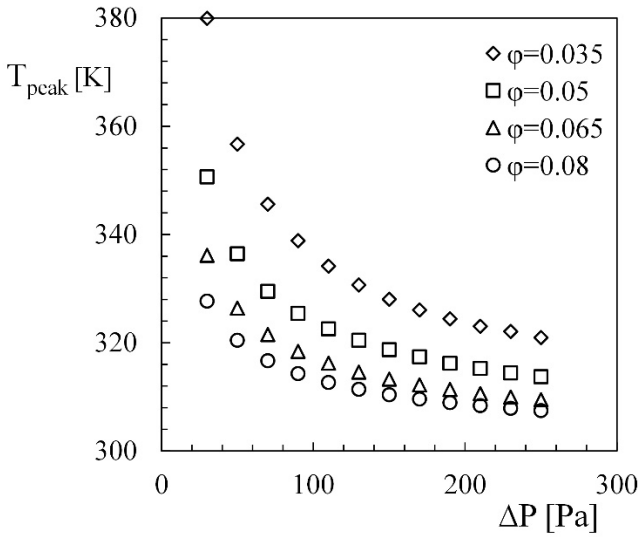

Figure 4.2. Peak temperature variation with pressure drop for radial design with volume fractions of φ=0.035, φ=0.05, 0.065 and 0.08

Next, consider the circular radial design with six and eight daughter channels in addition to ten, Figure 4.3. In order to have cooling channel diameters less than thickness of the plate, cooling performance of φ=0.05 and φ=0.035 are documented. Figure 4.3 shows that the flow resistances to the heat flow of radial design with six daughter channels are smaller than the design with eight and ten daughter channels as ΔP varies from 30Pa to 350Pa. This is expected due to the diameter of the cooling channels increase as the number of channels decreases, i.e., T_{peak} decreases as the number of channels decrease from 10 to 8 and 6. This means that for the specified volume fractions, the effects of the conductive resistances due to the spacing in between the channels are small enough in comparison with the effect of the convective resistances. Figure 4.3 also shows that the peak temperature decreases as the volume fraction increases. In addition, the comparison of the Figures 4.2 and 4.3 shows that the effect of the volume fraction and the number of channels on the peak temperature is more apparent with low pressure drops such as in

between 30Pa and 100Pa. Increasing the volume fraction and the number of channels in this pressure drop region can yield a change in the peak temperature. However, the volume fraction should be carefully increased in order to eliminate penetration of the plate walls by cooling channels.

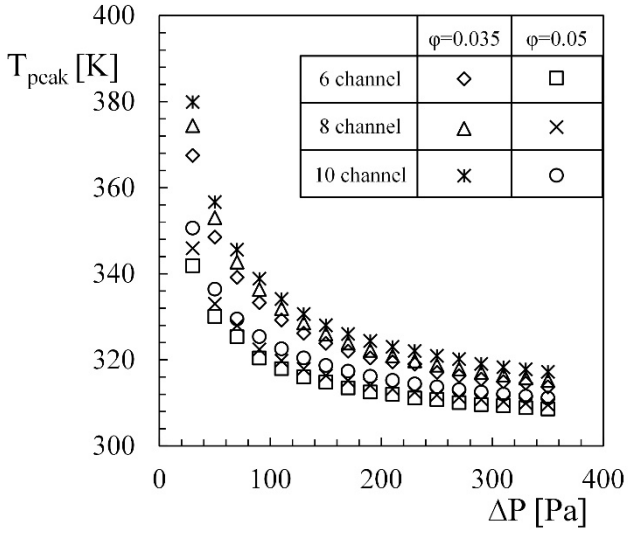

Figure 4.3. Peak temperature variation with pressure drop with 6, 8 and 10 number of channels when φ=0.035 and φ=0.05

4.1.2. Tree-shaped Design

Next, consider the tree-shaped design with three levels of embedded vascular cooling channels in Figure 4.4 with L=120mm, stainless steel plates and it is exposed to a heat load of 5000 W/m^2. The tree-shaped configurations are connected to one distributing and one collecting channels of diameter d_0. The coolant fluid enters from the distributing channel of diameter d_0, and then it is distributed to the vascular channels of diameter d_1, d_2 and d_3, respectively or vice versa. At the junctions, the channels of diameter d_1 bifurcate into two daughter channels of diameter d_2, then the channels of diameter d_2 bifurcate into two daughter channels of diameter d_3. Equation 4.1 gives the diameter ratio at the junctions, which is determined according to the Hess-Murray Rule (Bejan and Lorente, 2008).

$$d_i / d_{i+1} = 2^{1/3} \tag{4.1}$$

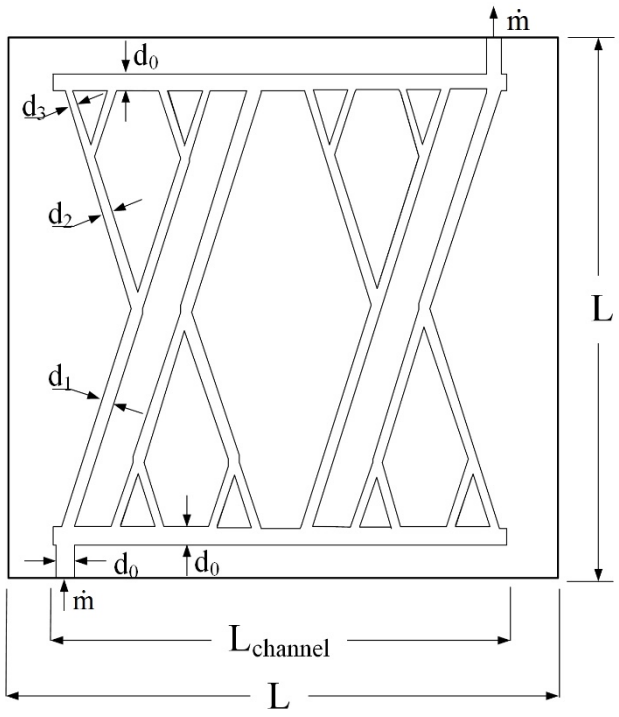

Figure 4.4. Tree-shaped design configuration

The resistances to the fluid flow decrease with the tree-shaped channel configuration, i.e. mass flow rate increases in between %9.25 to %18.9 in tree-shaped configurations in comparison to the radial configurations while pressure drop is fixed, which is in accord with the current literature (Bejan and Lorente, 2008; Lee et al., 2009; Rocha et al., 2009). Figure 4.5 (a) shows how the peak temperature varies relative to the pressure drop for two competing designs: radial and tree-shaped designs for φ=0.065 and φ=0.05. The peak temperature is the greatest with radial design when the pressure drop is 10 Pa for both volume fractions. However, the peak temperature of the radial design becomes smaller then tree-shaped design for a pressure drop range of 30 Pa to 290 Pa. Figure 4.5 (a) also shows that peak temperature increases while volume fraction decreases for both designs, which is in accord with Figures 4.2 and 4.3.

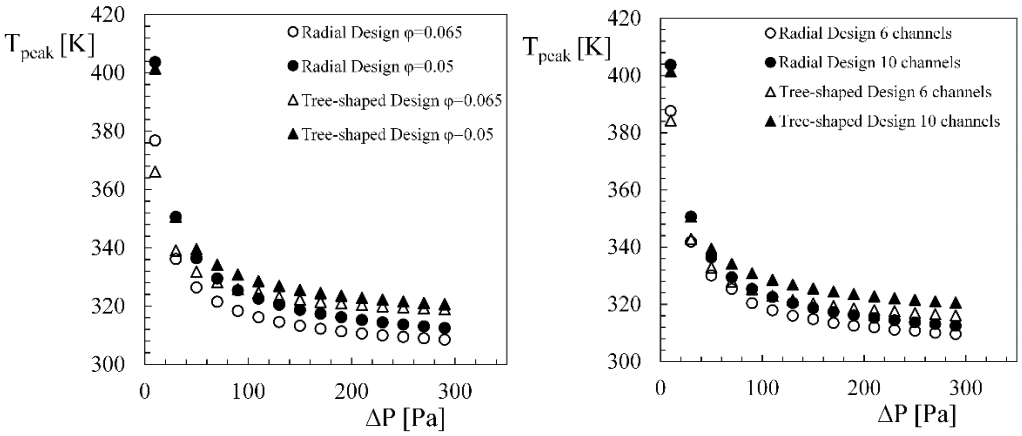

(a) (b)

Figure 4.5. Peak temperature relative to the pressure drop for tree-shaped and radial design for (a) 10 daughter channels with φ=0.065 and φ=0.05 (b) 6 and 10 daughter channels and with φ=0.05

In addition to the ten ports connected to the collecting and distributing channels, Figure 4.5 (b) also uncovers if there are six ports connected to the collecting and distributing channels, i.e., the effect of number of channels on peak temperature and the pressure drop. In radial design there are six parallel channels which are connected to the distributing and collecting channels of diameter d_0. The tree-shaped designs of one bifurcation level are also connected to the distributing and collecting channels of diameter d_0, i.e., the channels of diameter d_1 bifurcates into channels of diameter d_2 at the junctions (the channels of diameter d_3 is absent in Figure 4.4). The volume fraction was decreased from φ=0.065 to φ=0.05 in order to have smaller channel diameters than the thickness of the plate. Similar to Figure 4.5 (a), the peak temperature is smaller with tree-shaped design for a pressure drop of 10 Pa, and the peak temperature is smaller with radial design when pressure drop varies in between 30 Pa to 290 Pa. However, the effect of design governs the peak temperature and the effect of number of channels (from 6 to 10) and volume fraction (from 0.05 to 0.065) diminishes, Figure 4.5 (b).

4.1.3. Hybrid Design

The radial and tree-shaped designs are superior to each other because of the minimization of thermal and fluid flow resistances, respectively. Therefore, a hybrid of radial and tree-shaped designs is proposed to decrease both fluid and heat flow resistances in the order of their minimum values. Figure 4.6 shows the considered hybrid design.

Because the fluid flow and heat flow resistances are smaller and greater in tree-shaped designs then in radial designs, three additional radial channels of diameter d_2 is added to tree-shaped design. These added branches decrease the thermal resistances in between cooling channels to decrease peak temperature. Because the volume fraction is a constraint, the diameters of the vascular channels decrease with the additional branches. Even this decrease in the diameter increases the flow resistances, the uncooled regions are cooled with new branches. The desired vascular design should perform as good as radial design for cooling and tree-shaped design for pumping power requirements. Therefore, the design in Figure 4.6 is suggested, i.e., radial channels are placed in uncooled regions due to their superiority in cooling and tree-shaped channels are placed in cooled regions due to their low pumping power requirement.

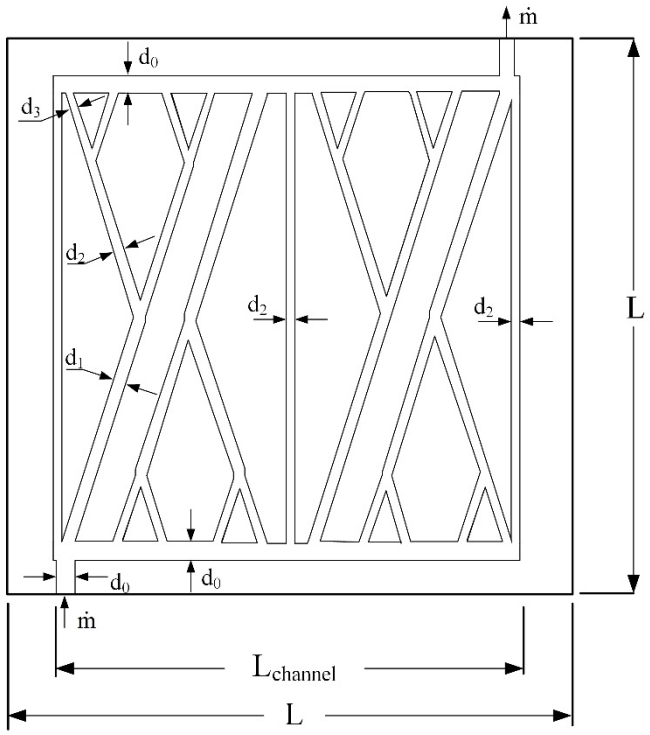

Figure 4.6. Hybrid design configuration

Figure 4.7 shows how the peak temperature varies relative to three competing designs: tree-shaped, radial and hybrid designs for the same volume fraction values. Tree-shaped design provides the smallest peak temperature at the pressure drop of 10 Pa, however, its value only 0.5% lower than the peak temperature of the hybrid design. Therefore, it can be concluded that hybrid designs perform almost as good as tree-shaped design when the fluid flow resistances govern the order of the peak temperature. Hybrid designs provide the smallest peak temperature when the pressure drop varies in between

30 Pa to 290 Pa. The difference between the peak temperature of the hybrid design and radial design decrease from 2.4% to 0.2% for 10 Pa and 290 Pa, respectively. This shows that as pressure drop increases, both radial and hybrid designs provides approximately the same temperature. Overall, Figure 4.7 shows that the peak temperature is the smallest or very close to the smallest with hybrid design for the entire pressure drop region for the given constraints and conditions.

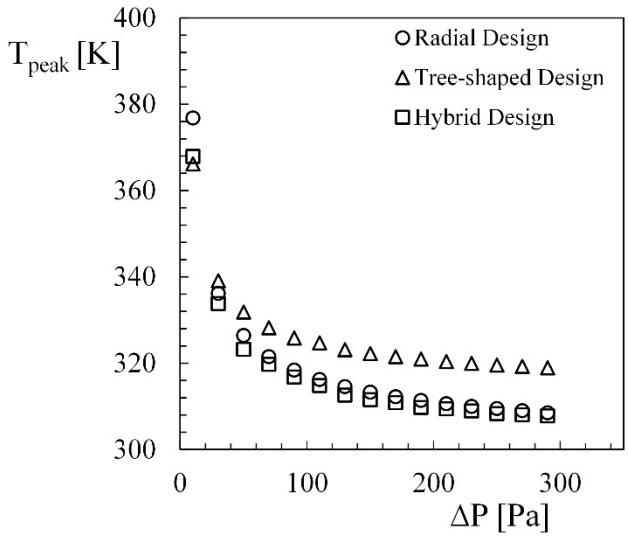

Figure 4.7. Peak temperature relative to the pressure drop for the competing designs for 10 daughter channels with φ=0.065

Figure 4.8 shows the temperature distribution on the top surface of the heated plate for the competing designs of radial (circular), tree-shaped and hybrid for 30 Pa and 290 Pa. Figures 4.8 (a), (c) and (e) show that the farthest locations to the inlet port reach to the peak temperature. In addition, because the flow rate of the coolant is low, the coolant fluid temperature rises to the undesired levels. Moreover, Figure 4.8 (c) shows that the hybrid design also promises the most uniform temperature distribution for 30 Pa. Figure 4.8 (b), (d) and (f) show the temperature distribution of the three competing designs for 290 Pa. Figure 4.8 (b) shows that the radial configuration promises to provide uniform temperature distribution with small disturbances at the farthest channels from the inlet ports. In addition, Figure 4.8 (d) shows that the temperature distribution is not uniform with tree-shaped channel configurations, i.e., the temperature is the smallest near the channel walls and it is the greatest in between and farther from the cooling channels. Therefore, even the fluid resistances are smaller in the tree-shaped design than in radial

design, the conductive resistances in between the channels govern the temperature distribution. Figure 4.8 (f) shows that the conductive thermal resistances can be decreased in between tree-shaped channels with embedded radial channels. Figure 4.8 (f) also shows that both the peak temperature is minimum and the temperature distribution is the uniform with hybrid designs for the given constraints and assumptions.

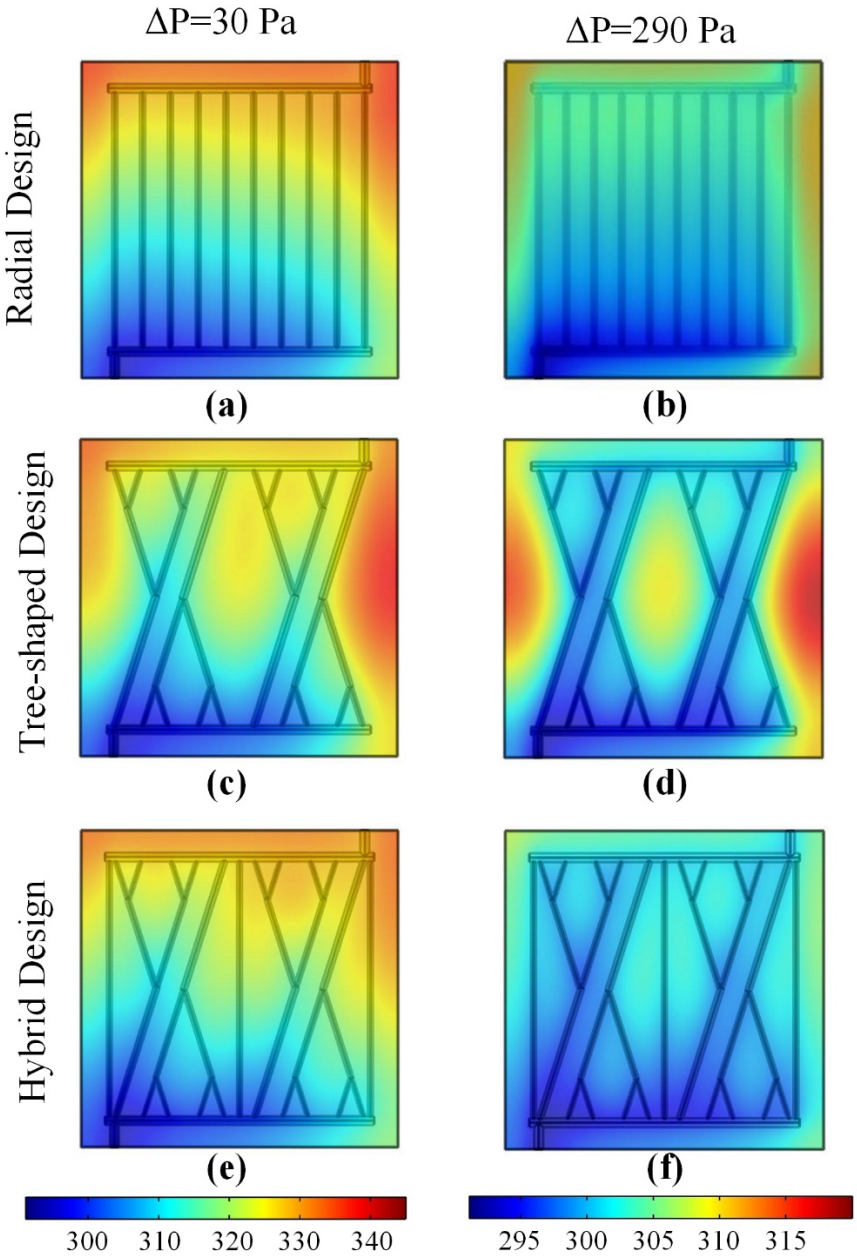

Figure 4.8. Temperature distribution of radial design for (a) 30 Pa, (b) 290 Pa, tree-shaped design for (c) 30 Pa, (d) 290 Pa, and hybrid design for (e) 30 Pa, (f) 290 Pa, for φ=0.065.

4.1.4. Time Dependent Study

Next, consider how the peak temperature evolves in time for the hybrid design shown in Figure 4.6. Three different inlet pressure condition were investigated: 30Pa, 150Pa and 290Pa as shown in Figure 4.9. In addition to governing equations that used in steady state case, $\partial\rho/\partial t$, $\rho\partial u/\partial t$, $\rho\partial v/\partial t$, $\rho\partial w/\partial t$ and $\rho c_p \partial T/\partial t$ terms are added to the left hand side of the conservation of mass, the conservation of momentum in x, y, z directions and the energy equation, respectively. Figure 4.9 shows that the required time for the peak temperature to reach steady state is decreased by increasing inlet pressure, P_{in}.

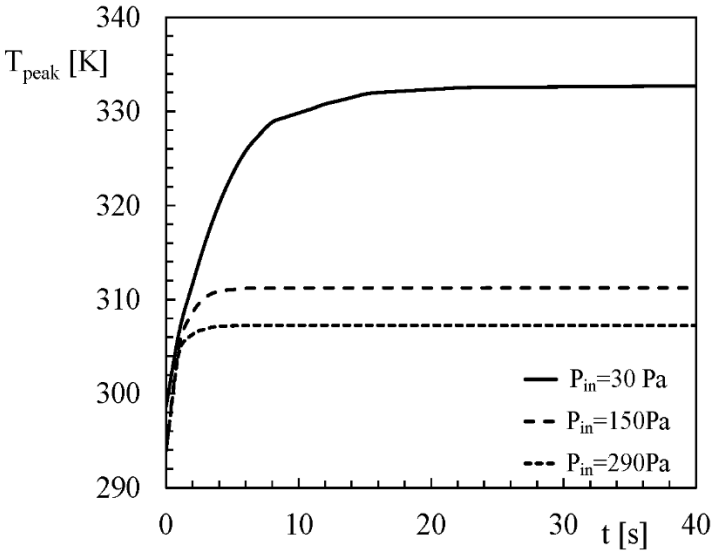

Figure 4.9. Peak temperature variation history for hybrid design: inlet pressures, 30, 150 and 290 Pa

In addition to uncovering the required time for the system to reach steady state, time dependent equations provides information on how long the working time of the pump can be delayed. Therefore, the boundary condition of the inlet surface is altered to

$$\Delta P = \begin{cases} 0 \; when \; t < t_d \\ P_{in} \; when \; t \geq t_d \end{cases} \tag{4.2}$$

where P_{in} is the constant inlet pressure difference, and t_d is the delayed time. Figure 4.10 (a) shows how the history of the peak temperature evolution with P_{in}=30 Pa for three t_d values: 5, 10 and 20 seconds. The effect of delaying the working time of the pump 5 seconds after applying the heating load, is negligibly small, i.e., peak temperature

increases 1.3% at t=5s. Increasing t_d also increases the order of the maximum peak temperature: peak temperature increases 6.2% and 16.4% as t_d becomes 10 and 20 seconds, respectively.

Figure 4.10 (b) shows the history of the peak temperature evolution when P_{in} is 150 Pa. Increasing P_{in} from 30Pa to 150Pa decreases the time required to reach steady state condition after $t = t_d$ time. Comparison of Figures 4.10 (a) and 10 (b) shows that the maximum peak temperature is almost the same. This is expected because the heat is stored in the plate until $t = t_d$. Therefore, it can be concluded that the maximum peak temperature is only the function of delayed time when the pump works with a delay. If the delay time is low such as 5 seconds, the order of the maximum peak temperature at $t = t_d$ is almost the same as the steady state peak temperature. However, increasing t_d and ΔP increases the difference between the maximum peak temperature at $t=t_d$ and the peak temperature at $t \gg t_d$, respectively.

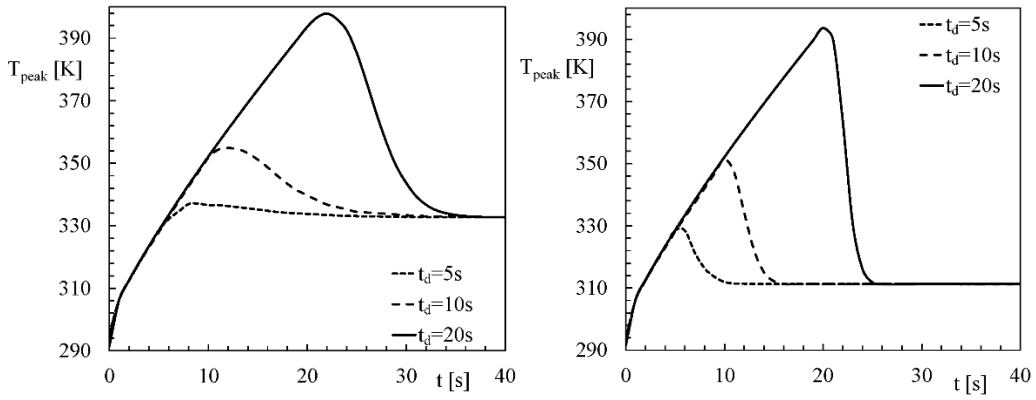

(a) (b)

Figure 4.10. The evolution of peak temperature for hybrid design: when inlet pressure is a function of time for (a) 30Pa and (b) for 150Pa

4.2. 170x170 Vascular Plates

In this section, the experimental procedure that explained in Chapter 3 is conducted with 170x170mm vascular plates in order to validate the numerical results.

The results are documented as peak temperature relative to pressure drop and temperature distributions of the plates.

4.2.1. Radial Design

Next, consider the radial cooling channel design with 170x170mm Aluminum vascularized plates with volume fraction of φ=0.05. Figure 4.11 documents the relation between the peak temperature and the pressure drop for experimental and numerical studies. The experimental procedure was discussed in Chapter 3, and the considered heating loads are 50W and 150W. Figure 4.11 shows that the results of the numerical and experimental studies agree, the maximum relative errors are 0.88% and 0.39% for 50W and 150W, respectively. In addition, these differences are in between the calculated values in uncertainty analysis. The volumetric flow rate is limited as to $7x10^{-6}$ m^3/s, therefore, the flow is laminar. In addition, increasing the pressure drop after 350 Pa does not decrease the peak temperature more than several percent as discussed in the numerical results of Figure 4.1 (b).

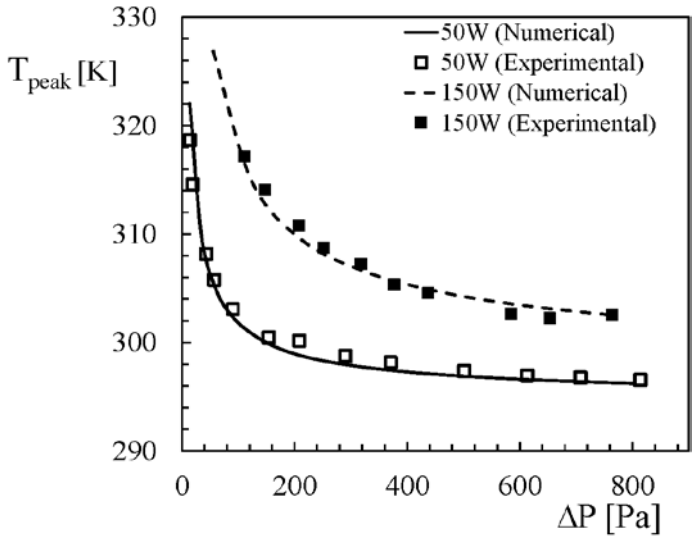

Figure 4.11. Peak temperatures relative to pressure drop for experimental and numerical studies of radial design for heat loads of 50W and 150W

Figure 4.12 illustrates the temperature distributions of the numerical and experimental studies, for two heating loads: 50W and 150W. Similar to Figure 4.11, both Figures 4.12 (a) and 4.12 (b) shows the agreement between the numerical and experimental studies. In addition, Figure 4.12 (a) shows that the peak temperature on the

vascular plate surface are located close to the outlet channel for low volumetric flow rates. Because the time required for the coolant fluid to reach to those region, the temperature of the coolant fluid was already increased, therefore it cannot cool the vascular plate down. In Figure 4.12 (b), the hot spots are both located in the middle of the plate close to the collecting channel.

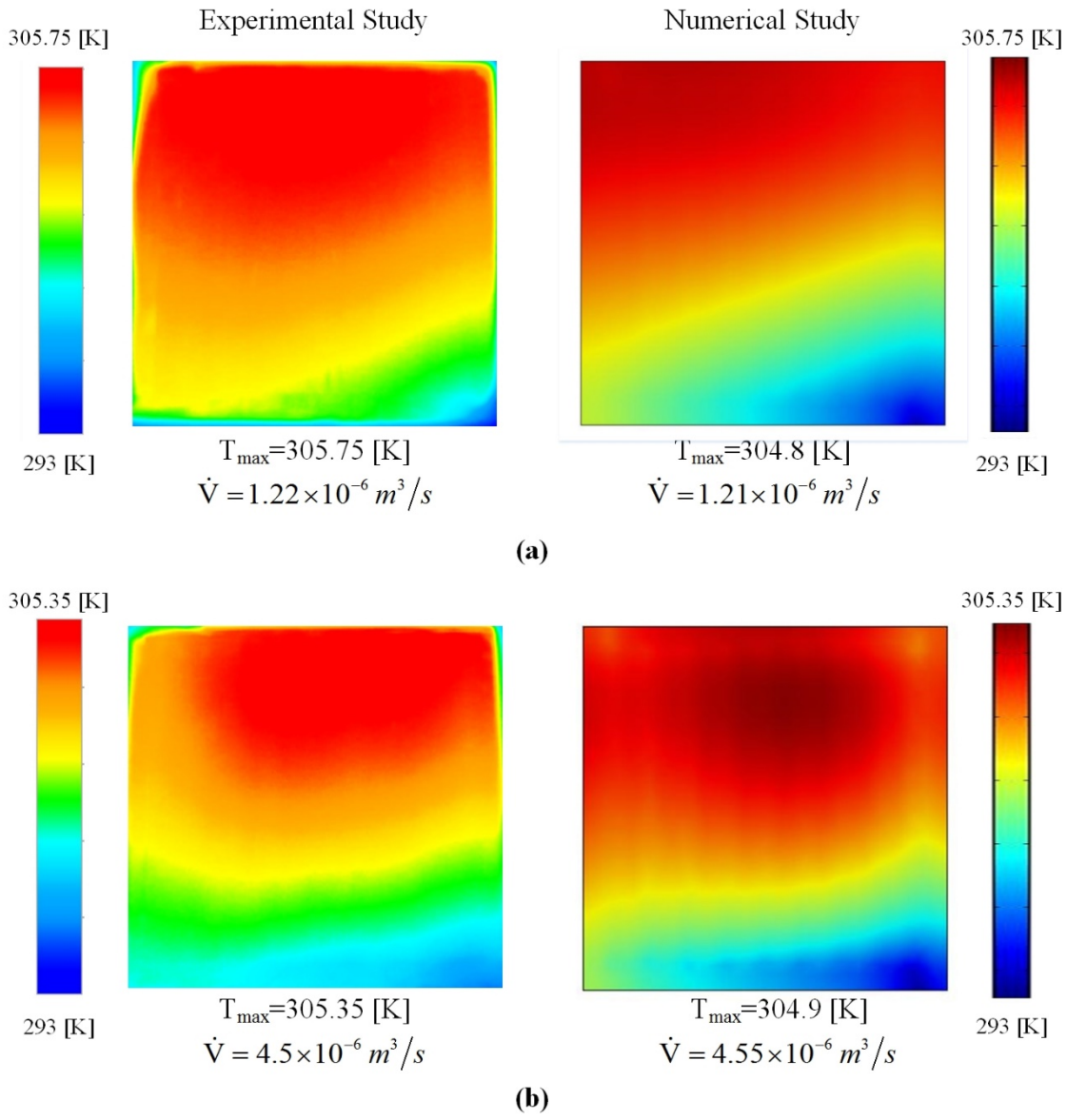

Figure 4.12. Comparison of temperature distributions of radial design for experimental and numerical studies with (a) 50W (b) 150W of heating loads

4.2.2. Tree-shaped Design

Figure 4.13 shows how the peak temperature varies relative to the pressure drop for tree-shaped design with 170x170mm Aluminum vascular plates for heating loads of 50W and 150W. The results of experimental and numerical studies are in agreement, i.e., 0.49% and 0.23% maximum relative errors on peak temperature for 50W and 150W, respectively. In addition, Figure 4.14 shows the temperature distributions of the tree-shaped design, for experimental and numerical studies for two heating loads. For $\dot{V}$=1.27x10^{-6} m^3/s, the temperature distribution is similar with the radial design, the peak temperatures are located around collecting channels. However, for $\dot{V}$=4.54x10^{-6} m^3/s, the peak temperatures are located in between the tree-shaped channels where there is no embedded cooling channels. This result shows that conductive resistances becomes essential as the pressure drop increases.

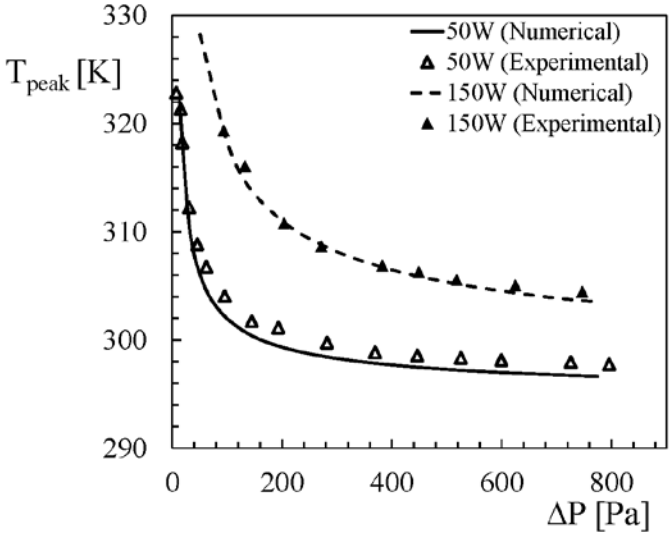

Figure 4.13. Peak temperatures relative to pressure drop for experimental and numerical studies of tree-shaped design for heat loads of 50W and 150W

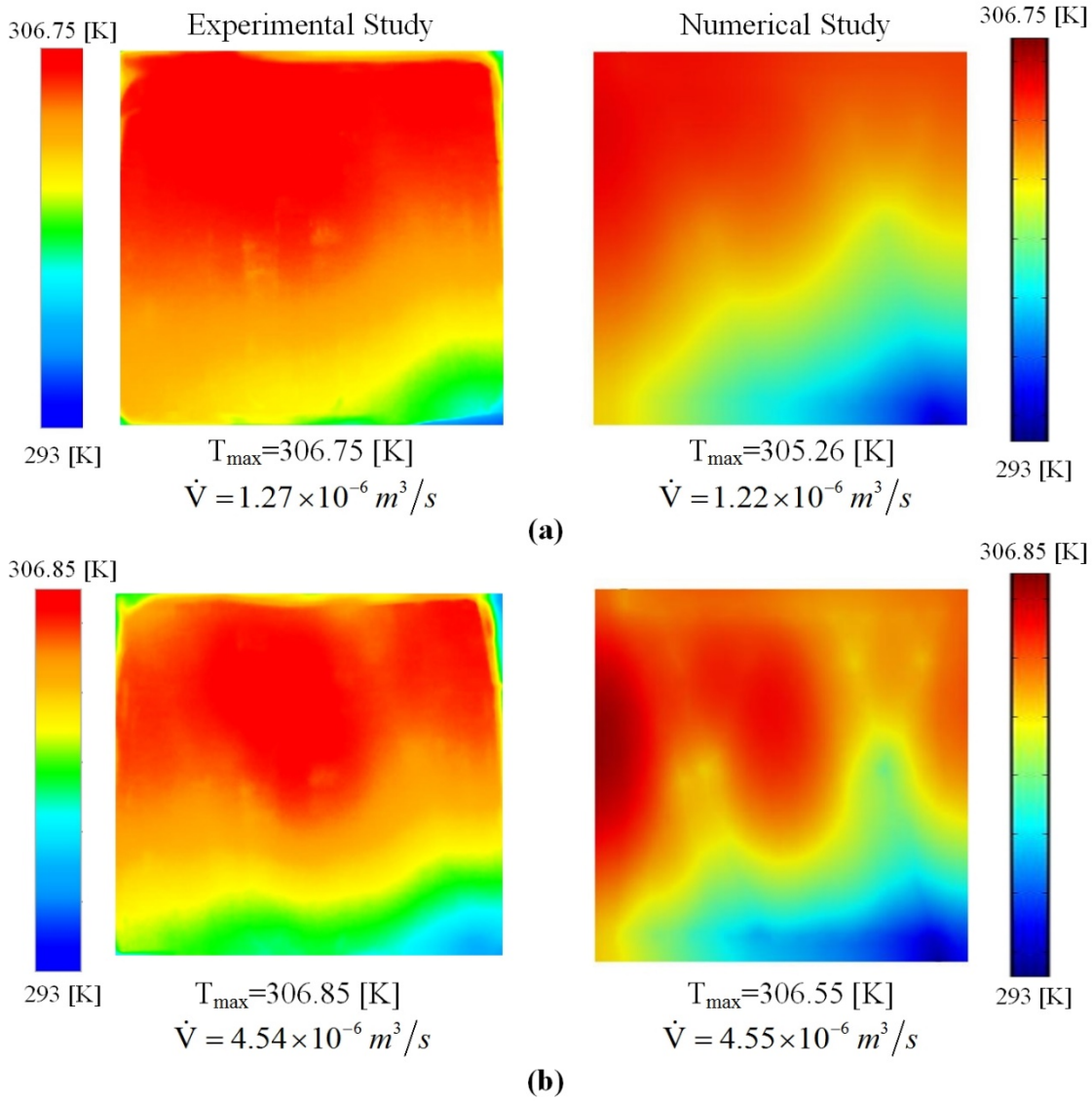

Figure 4.14. Comparison of temperature distributions of tree-shaped design for experimental and numerical studies with (a) 50W (b) 150W of heating loads

4.2.3. Hybrid Design

Consider the hybrid design of Figure 12 made of Aluminum with the plate size of 170x170mm. Figure 4.15 shows the thermal performance of the hybrid design for both experimental and numerical studies for two different heat loads (50W and 150W). The comparison shows that there is a good agreement (0.94% and 0.22% maximum relative errors between experimental and numerical studies, for 50W and 150W of heat loads, respectively), since these differences are in between the calculated values in uncertainty

analysis. Also, the peak temperature does not decrease more than several percent when the pressure drop is higher than 200 Pa.

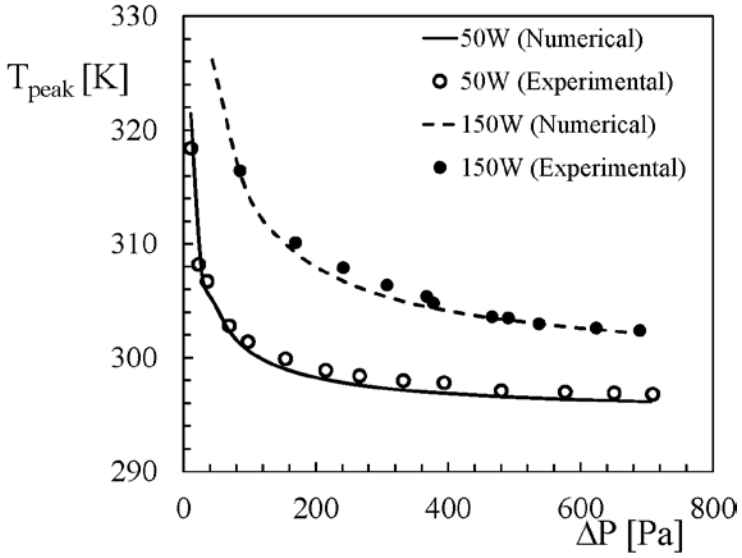

Figure 4.15. Peak temperatures against pressure drop for experimental and numerical studies of hybrid design for heat loads of 50W and 150W

Next, Figure 4.16 shows the temperature distributions of numerical and experimental study for 50W and 150W heat loads. In Fig. 4.16 (a), it is same as radial and tree-shaped design, the hot spots are located near to outlet channel, since the volumetric flow rate is small and thus coolant fluid cannot reach the outlet channel without heating up, also the temperature patterns are similar in both numerical and experimental study. Furthermore, Fig. 4.16 (b) shows the peak temperature is close to the collecting channel in the middle, both in experimental and numerical results. In order to eliminate the peak temperature located in the middle, diameter of additional channels should be increased in 170x170mm plates.

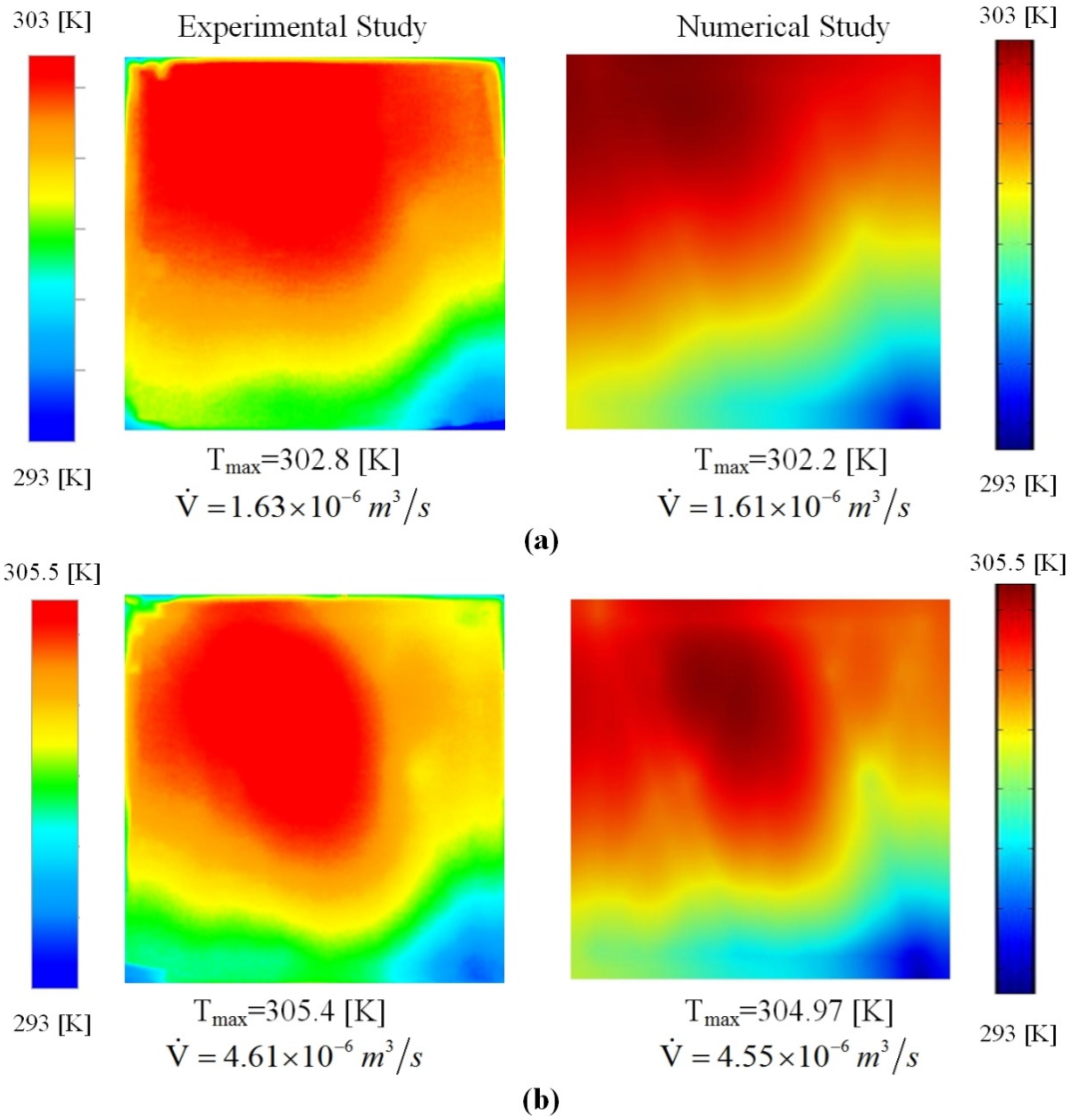

Figure 4.16. Comparison of temperature distributions of hybrid design for experimental and numerical studies with (a) 50W (b) 150W of heating loads

Figure 4.17 shows the comparison of the thermal performances of the three competing designs; radial, tree-shaped and hybrid designs, with (a) Aluminum 170x170mm vascular plates and (b) Stainless Steel 170x170mm vascular plates, when the heat load is 50W. Figure 4.17 (a) documents that by means of peak temperature hybrid design performs slightly better than other designs, which is more significant when the pressure drop is changing from 40Pa to 400Pa (peak temperatures are 1% lower), after that point design effect diminishes and all designs performs almost the same (the peak temperature changes less than %0.01) due to the effect of convective resistances becomes negligibly small in comparison with the conductive resistances.

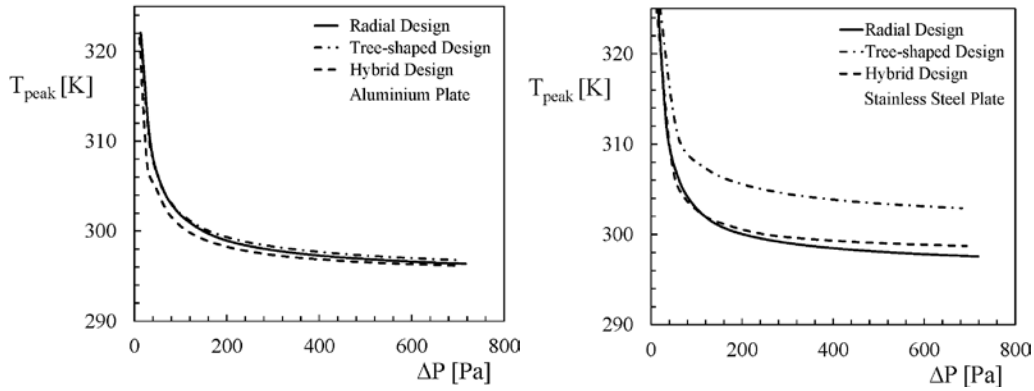

(a) (b)

Figure 4.17. Peak temperatures relative to the pressure drop for the the competing designs with (a) Aluminum plates and (b) Stainless Steel plates

In order to uncover the effect of material on the thermal performance for the competing designs, the studies were repeated for AISI-304 stainless steel. Figure 4.17 (b) shows how the peak temperature varies relative to the pressure drop for stainless steel vascular plates. Unlike in Figure 4.17 (a), Figure 4.17 (b) shows that the effect of design on the peak temperature is visible, i.e., tree-shaped design has 1.8% and 1.5% greater peak temperatures in comparison to radial and hybrid designs, respectively. The reason for this change is due to the increase in the conductive thermal resistances (thermal conductivity of stainless steel is almost twenty times less than Aluminum). Therefore, the effect of uncooled regions creates a non-uniform temperature distribution in the tree-shaped design in comparison to the other designs. The thermal performance of radial design is slightly better than the performance of the hybrid design (peak temperature is 0.5% less) as pressure drop becomes more than 100 Pa. When the pressure drop is less than 100 Pa, the peak temperature is minimum with hybrid design as shown in Fig. 4.17 (a) and (b). For the same pressure drop value, flow rate is greater in the hybrid design than in the radial design. Therefore, the peak temperature is minimum with the hybrid design when the pressure drop is less than 100 Pa, even though the conductive resistances are greater in the hybrid design than in the radial design.

CHAPTER 5

CONCLUSION

Here, we showed that a plate with applied heating load on one of its surfaces can be kept under a desired temperature level with embedded cooling channels both numerically and experimentally. The effect of the cross-section of the vascular channels on the cooling performance is uncovered for radial channel configuration. Circular channels provide greater cooling performance when the pressure drop is smaller (up to 1000 Pa). The semi-circular radial channels provide slightly better cooling performance (0.1% lower peak temperature) than circular channels as the pressure drop is in the order of 3000 Pa. The effect of the volume fraction and the number of channels on cooling performance for radial design are documented, i.e., the peak temperature decreases as φ increases, and decreasing the number of channels from 10 to 6 when φ=0.05, 0.035 decreases the peak temperature. In addition, an experimental procedure is applied and the results are compared with numerical results, and the maximum relative error is 0.88% for peak temperatures on the top surface. In addition, temperature distributions are compared in Fig. 4.12 and it's indicated that there is good agreement between experimental and numerical results.

Then, the effect of changing the design from the radial configuration to tree-shaped configuration is uncovered with fixed volume fraction. Tree-shaped configurations provide smaller flow resistances than the radial configurations. Therefore, the peak temperature is minimum with tree-shaped configurations when the pressure drop is small (i.e., 10 Pa as in shown in Fig. 4.5). However, conductive thermal resistances are greater in tree-shaped configurations than in radial configurations. Therefore, radial configurations provide better cooling performance as the pressure drop increases. In addition, experimental results of tree-shaped design is compared with numerical results, for peak temperatures on the top surface and the temperature distributions. Again there is a good agreement between the experimental and numerical results, the maximum relative error is 0.49%.

All these results lead us to suggest a hybrid design of radial and tree-shaped configurations. This hybrid design is created by inserting radial channels in between tree-

shaped channels. This hybrid design provides the smallest peak temperature (or very close to the smallest peak temperature), Fig. 4.7, for the entire pressure drop region and most uniform temperature distribution, Fig. 4.8. Then, how the peak temperature of the hybrid design affected by the time is investigated for different inlet pressures. How long it takes to reach steady state condition is documented. Then, time dependent study of hybrid design with delayed cooling was considered. Varying the delay time affects the peak temperature at $t=t_d$, which is the maximum peak temperature. Increasing ΔP decreases the required time to reach steady state condition and the peak temperature at steady state conditions ($t \gg t_d$).

Then, the thermo-fluidic performance of the hybrid design that we suggested is investigated experimentally and compared with numerical results, the maximum relative error was 0.94%, which shows there is an agreement between numerical and experimental results. Furthermore, 170x170mm vascular plates are simulated for stainless steel in order to uncover the materials effect on cooling performance. Increase in conductive resistances due to the thermal conductivity decrease made it more clear the design effect on thermal performances. And it is safe to say that there is no best design, there are best designs for different boundary conditions.

Overall, this work shows how a plate can be vascularized for enhancing the thermal conductance. The results were validated with experiments, and the effect of material on the thermal performance and optimum vascular channel design selection were covered. Here we showed that each design is superior to the others for a specific set of objective and conditions.

REFERENCES

BEJAN, A. 1996. Constructal-theory network of conducting paths. *International Journal of Heat and Mass Transfer,* 40**,** 799-816.

BEJAN, A., LORENTE, S. & WANG, K. M. 2006. Networks of channels for self-healing composite materials. *Journal of Applied Physics,* 100**,** 033528.

BEJAN, A., LORENTE, S. 2006. Constructal theory of generation of configuration in nature and engineering. *Journal of Applied Physics,* 100**,** 041301.

BEJAN, A., LORENTE, S. 2008. *Design with Constructal Theory,* John Wiley & Sons, Inc.

BEJAN, A., LORENTE, S. 2013. Constructal law of design and evolution: Physics, biology, technology, and society. *Journal of Applied Physics,* 113**,** 151301.

BELLO-OCHENDE, T., LIEBENBERG, L. & MEYER, J. P. 2007. Constructal cooling channels for micro-channel heat sinks. *International Journal of Heat and Mass Transfer,* 50**,** 4141-4150.

CETKIN, E. 2015. Constructal Vascular Structures With High-Conductivity Inserts for Self-Cooling. *Journal of Heat Transfer,* 137**,** 111901.

CETKIN, E., LORENTE, S. & BEJAN, A. 2011a. Hybrid grid and tree structures for cooling and mechanical strength. *Journal of Applied Physics,* 110**,** 064910.

CETKIN, E., LORENTE, S. & BEJAN, A. 2011b. Vascularization for cooling and mechanical strength. *International Journal of Heat and Mass Transfer,* 54**,** 2774-2781.

CETKIN, E., LORENTE, S. & BEJAN, A. 2012. Vascularization for cooling a plate heated by a randomly moving source. *Journal of Applied Physics,* 112**,** 084906.

CETKIN, E., LORENTE, S. & BEJAN, A. 2015. Vascularization for cooling and reduced thermal stresses. *International Journal of Heat and Mass Transfer,* 80**,** 858-864.

CETKIN, E., OLIANI, A. 2015. The natural emergence of asymmetric tree-shaped pathways for cooling of a non-uniformly heated domain. *Journal of Applied Physics,* 118**,** 024902.

CHO, K.-H. CHAN, W.-P.; KIM, M.-H. 2011. A numerical and experimental study to evaluate performance of vascularized cooling plates. *International Journal of Heat and Fluid Flow,* 32**,** 1186-1198.

CHO, K.-H. LEE, J.; AHN, H. S.; BEJAN, A.; KIM, M. H. 2010. Fluid flow and heat transfer in vascularized cooling plates. *International Journal of Heat and Mass Transfer,* 53**,** 3607-3614.

FIGLIOLA, R. S., BEASLEY, D.E. 2011. *Theory and Design for Mechanical Measurements*, John Wiley & Sons, Inc.

KIM, S., LORENTE, S. & BEJAN, A. 2006. Vascularized materials: Tree-shaped flow architectures matched canopy to canopy. *Journal of Applied Physics,* 100**,** 063525.

KIM, S., LORENTE, S. & BEJAN, A. 2008. Dendritic vascularization for countering intense heating from the side. *International Journal of Heat and Mass Transfer,* 51**,** 5877-5886.

KOBAYASHI, H., LORENTE, S., ANDERSON, R. & BEJAN, A. 2013. Trees and serpentines in a conducting body. *International Journal of Heat and Mass Transfer,* 56**,** 488-494.

LEE, J., KIM, S., LORENTE, S. & BEJAN, A. 2008. Vascularization with trees matched canopy to canopy: Diagonal channels with multiple sizes. *International Journal of Heat and Mass Transfer,* 51**,** 2029-2040.

LEE, J., LORENTE, S. & BEJAN, A. 2009. Transient cooling response of smart vascular materials for self-cooling. *Journal of Applied Physics,* 105**,** 064904.

MA, T. Y., H.; ZHANG, Y.; LU, L.; WANG, X. 2015. Using phase change materials in photovoltaic systems for thermal regulation and electrical efficiency improvement: A review and outlook. *Renewable and Sustainable Energy Reviews,* 43**,** 1273-1284.

MINEA, A. A. 2015. Numerical studies on heat transfer enhancement and synergy analysis on few metal oxide water based nanofluids. *International Journal of Heat and Mass Transfer,* 89**,** 1207-1215.

MOREGA, A. M. O., J.C.; NEGOIAS, P.A.; MOREGA, M.; HOVSAPIAN, R. 2006. Optimal Electrical Design of Spherical Photovoltaic Cells. *COMSOL Conference.* Czech Technical University Prague.

ODOM, S. A. TYLER, T.P., CARUSO, M.M., RITCHEY, J.A., SCHULMERICH, M.V., ROBINSON, S.J., BHARGAVA, R., SOTTOS, N.R., WHITE, S.R., HERSAM, M.C., MOORE, J.S. 2012. Autonomic restoration of electrical conductivity using polymer-stabilized carbon nanotube and graphene microcapsules. *Applied Physics Letters,* 101**,** 043106.

RAJA, V. A. P., BASAK, T., DAS, S. K. 2008. Thermal performance of a multi-block heat exchanger designed on the basis of Bejan's constructal theory. *International Journal of Heat and Mass Transfer,* 51**,** 3582-3594.

ROCHA, L. A. O., LORENTE, S. & BEJAN, A. 2009. Tree-shaped vascular wall designs for localized intense cooling. *International Journal of Heat and Mass Transfer,* 52**,** 4535-4544.

SCIACOVELLI, A., VERDA, V. 2011. Entropy Generation Minimization for the Optimal Design of the Fluid Distribution System in a Circular MCFC. *International Journal of Thermodynamics,* 14.

SHAFAHI, M., BIANCO, V., VAFAI, K. & MANCA, O. 2010. Thermal performance of flat-shaped heat pipes using nanofluids. *International Journal of Heat and Mass Transfer,* 53**,** 1438-1445.

SOGHRATI, S., THAKRE, P. R., WHITE, S. R., SOTTOS, N. R. & GEUBELLE, P. H. 2012. Computational modeling and design of actively-cooled microvascular materials. *International Journal of Heat and Mass Transfer,* 55**,** 5309-5321.

THERRIAULT, D., WHITE, S. R. & LEWIS, J. A. 2003. Chaotic mixing in three-dimensional microvascular networks fabricated by direct-write assembly. *Nature Materials,* 2**,** 265-71.

TOOHEY, K. S., SOTTOS, N. R., LEWIS, J. A., MOORE, J. S. & WHITE, S. R. 2007. Self-healing materials with microvascular networks. *Nature Materials,* 6**,** 581-5.

WANG, K. M., LORENTE, S. & BEJAN, A. 2009. Vascular materials cooled with grids and radial channels. *International Journal of Heat and Mass Transfer,* 52**,** 1230-1239.

WANG, K. M., LORENTE, S. & BEJAN, A. 2010. Vascular structures for volumetric cooling and mechanical strength. *Journal of Applied Physics,* 107**,** 044901.

WHITE, S. R., SOTTOS, N.R., GEUBELLE, P.H., MOORE, J.S., KESSLER, M.R., SRIRAM, S.R., BROWN, E.N., VISWANATHAN, S. 2001. Autonomic Healing of Polymer Composites. *Nature,* 409**,** 794-797.